



OPEN ACCESS

EDITED BY

Jason Lanoue,
Agriculture and Agri-Food Canada (AAFC),
Canada

REVIEWED BY

Ali Baghdadi,
University of Saskatchewan, Canada
Telesphore R. J. G. Marie,
Queen's University, Canada
Yanwei Liu,
Kunming University of Science and
Technology, China

*CORRESPONDENCE

Rhuanito Soranz Ferrarezi
✉ ferrarezi@uga.edu

RECEIVED 28 October 2025

REVISED 07 January 2026

ACCEPTED 15 January 2026

PUBLISHED 10 February 2026

CITATION

Nam S and Ferrarezi RS (2026) Real-time chlorophyll fluorescence monitoring reveals dynamic acclimation of lettuce to temperature and light stress in controlled environments.

Front. Plant Sci. 17:1733839.

doi: 10.3389/fpls.2026.1733839

COPYRIGHT

© 2026 Nam and Ferrarezi. This is an open-access article distributed under the terms of the [Creative Commons Attribution License \(CC BY\)](https://creativecommons.org/licenses/by/4.0/). The use, distribution or reproduction in other forums is permitted, provided the original author(s) and the copyright owner(s) are credited and that the original publication in this journal is cited, in accordance with accepted academic practice. No use, distribution or reproduction is permitted which does not comply with these terms.

Real-time chlorophyll fluorescence monitoring reveals dynamic acclimation of lettuce to temperature and light stress in controlled environments

Suyun Nam and Rhuanito Soranz Ferrarezi*

Department of Horticulture, University of Georgia, Athens, GA, United States

Real-time monitoring of photosynthetic efficiency can improve our understanding of plant stress responses. In this study, we used a high-frequency chlorophyll fluorescence (CF) monitoring system to investigate the effects of combined temperature and light effects on lettuce. Plants were exposed to three temperatures (18, 25, and 32 °C) and two light intensities (150 and 500 $\mu\text{mol}\cdot\text{m}^{-2}\cdot\text{s}^{-1}$) for one week, and CF parameters were measured every 30 minutes. Gas exchange measurements were conducted at 2 and 7 days after treatment (DAT). High light combined with low temperature initially suppressed Φ_{PSII} but gradually improved via reductions in quantum yield of non-regulated energy dissipation (Φ_{NO}), indicating adjustments in the photosynthetic machinery. While the quantum yield of non-photochemical quenching (Φ_{NPQ}) decreased sharply only on the first day, Φ_{NO} continued to decline, highlighting its role in longer-term acclimation. In contrast, high temperatures enhanced CO_2 assimilation through elevated stomatal conductance; however, the maximum efficiency of PSII (F_v/F_m) remained suppressed (~ 0.81), suggesting sustained photoinhibition. The relationship between electron transport rate (ETR) and photosynthetic rate (A) varied with temperature and time, indicating that the efficiency of converting photochemical energy into carbon assimilation depended on stress conditions and the acclimation stage. However, cumulative ETR integrated over the experiment period was significantly associated with shoot dry weight independent of temperature conditions, indicating that temporally integrated CF metrics retain predictive value for growth, unlike instantaneous CF parameters. These findings demonstrate that high-resolution CF monitoring captures subtle and dynamic photosynthetic responses that are not detectable via single-point gas exchange measurements alone. The ability to interpret changes in CF parameters in real-time provides valuable insights into plant acclimation and stress physiology for the optimization of environmental conditions in controlled environment agriculture systems.

KEYWORDS

abiotic stress, chlorophyll fluorescence, controlled environment agriculture, light acclimation, photosynthetic efficiency, temperature stress

1 Introduction

Maintaining optimal photosynthetic performance in controlled environment agriculture (CEA) facilities is challenging under overcast or substandard environmental conditions. Limited or excessive light and temperature can induce physiological stress and increase reliance on energy-intensive environmental control, including supplemental lighting, shading systems, and heating, ventilation, and air conditioning (HVAC) systems. Therefore, optimizing photosynthetic efficiency is critical for maximizing crop productivity and improving energy use efficiency in CEA. High light intensity and temperature stress are among the most common environmental constraints in CEA production systems (Zhou et al., 2022). In general, photosynthetic efficiency decreases under excessive light, because surplus absorbed light energy is dissipated as heat and chlorophyll fluorescence to prevent photodamage to photosystem II (PSII) (Wimalasekera, 2019). Both heat and cold stress reduce photosynthetic efficiency and impair plant growth, primarily through the generation of reactive oxygen species (ROS) and photodamage to PSII components (Hussain, 2019).

However, the effect of high light and temperature stress varies depending on the combination of stressors and the duration of exposure. In particular, low temperatures combined with high light intensities can synergistically induce severe photoinhibition due to the overexcitation of PSII reaction centers (Janda et al., 2021). Prolonged exposure to both high light and high temperatures may lead to the irreversible inactivation of PSII due to the downregulation of PSII protein gene expression and associated repair mechanisms (Lu et al., 2017). Although this combination of stressors can mitigate oxidative damage through the accumulation of carbohydrates and carotenoids as protective and adaptive strategies, its effectiveness depends on the severity of the stresses and the crop species (Zhou et al., 2020).

Moreover, the stress responses are crop-specific and evolve over time, influenced by “stress memory”, defined as a history of exposure to different types of environmental stresses (Bruce et al., 2007; Yamori et al., 2014). For instance, the photosynthetic efficiency of lettuce (*Lactuca sativa*) increased significantly within a single day under high light, whereas cucumber (*Cucumis sativus*) maintained a constant level, indicating a species-specific response (Nam et al., 2025). Over longer periods, plants exhibit dynamic acclimation to light and temperature stresses through diverse physiological mechanisms such as chloroplast relocation, accumulation of accessory pigments, membrane fluidity adjustments, and leaf morphological changes (Wimalasekera, 2019). Monitoring real-time plant stress responses is essential for understanding how environmental factors dynamically influence photosynthetic performance. While single-leaf gas exchange remains a conventional method for assessing photosynthetic capacity and stomatal behavior, it is time-consuming and not suitable for high-frequency or long-term real-time monitoring. Consequently, temporal dynamics and acclimation patterns are often overlooked (Haworth et al., 2023). Whole-plant gas exchange systems enable the continuous measurement of whole-canopy photosynthesis, but their complexity reduces their practical applicability (Sakoda et al., 2025;

van Iersel and Bugbee, 2000). Other traditional physiological assessments, such as biochemical or pigment analyses, are labor-intensive and destructive. Even though these more sophisticated systems have limited use, high-temporal-resolution monitoring is therefore critical for early stress detection, capturing within-day and long-term variability, and improving our understanding of plant-environment interactions (Haworth et al., 2023).

Chlorophyll fluorescence (CF) monitoring, based on the pulse amplitude modulation (PAM) technique, is a rapid, non-destructive, and highly sensitive method for detecting environmental stress. Parameters such as the maximum efficiency of PSII (F_v/F_m) serve as diagnostic indicators of photoinhibition under extreme temperature or excess light (Lysenko et al., 2022). Because CF measurements are non-destructive, repeated sampling enables detection of diurnal changes and acclimation responses. Linear electron transport rate (ETR) is generally well correlated with carbon dioxide (CO₂) assimilation, offering a potential proxy for crop productivity. Additionally, CF allows detailed analysis of dynamic photochemical quenching, including regulated and unregulated energy dissipation (Lysenko et al., 2022; Maxwell and Johnson, 2000).

CF has been applied for early abiotic stress detection, crop phenotyping, prediction of flowering time, and development of productivity models (Hussain, 2019; Kalaji et al., 2016; Yu and Chen, 2023). It has also been implemented in real-time environmental control systems for artificial lighting. For example, a CF-based biofeedback system can collect CF parameters every 15 minutes via serial communication with a datalogger to dynamically adjust the lighting-emitting diode (LED) light intensity (Nam et al., 2025; van Iersel et al., 2016).

However, under photorespiratory stress conditions such as heat or drought, the relationship between ETR and carbon assimilation may weaken due to low CO₂ availability (Lysenko et al., 2022). This can cause a decoupling between fluorescence parameters and the actual carbon assimilation, which may limit the reliability of CF as a proxy for photosynthetic performance under certain stressful conditions. This response should be better studied to understand the factors needed to control lighting successfully.

The overall objective of this study was to demonstrate the utility of a high-frequency CF monitoring system for assessing plant physiological responses under temperature and light stress over time. It was hypothesized that high-frequency CF measurements can resolve temperature- and light-dependent stress responses and their interaction and acclimation dynamics over time, and that CF-derived metrics are associated with downstream physiological outcomes, including carbon assimilation and crop growth under stress conditions. This knowledge can be used for further automated lighting control using CF as a biofeedback control system.

2 Materials and methods

2.1 Location

The study was conducted at the University of Georgia (College of Agricultural and Environmental Sciences, Department of

Horticulture, Controlled Environment Agriculture Crop Physiology and Production Laboratory) in Athens, Georgia, USA (33° 93' 11.36" N, 83° 36' 39.28" W).

2.2 Plant material, growth conditions

Lettuce 'Green Towers' seeds (Johnny's Selected Seeds, Waterville, ME, USA) were sown into 10-cm square containers filled with a peat-perlite soilless substrate (Fafard 1P; SunGro Horticulture, Agawam, MA, USA). Seedlings were grown in a walk-in growth chamber illuminated with white LED light bars (RAY series with Physiospec indoor spectrum; Fluence Bioengineering, Austin, TX, USA) emitting 39% red, 40% green, 18% blue, and 3% far-red. Canopy-level photosynthetic photon flux density (PPFD) was maintained at 250 $\mu\text{mol}\cdot\text{m}^{-2}\cdot\text{s}^{-1}$, with a 16-h photoperiod (daily light integral [DLI] of 14.4 $\text{mol}\cdot\text{m}^{-2}\cdot\text{d}^{-1}$). Irrigation was supplied daily by an automated ebb-and-flow subirrigation system using a 15N-2.2P-12.4K fertilizer (Jack's Professional[®] LX 15-5-15 Cal-Mg LX; JR Peters, Allentown, PA, USA) at 100 $\text{mg}\cdot\text{L}^{-1}$ N. The average environmental conditions were a temperature of 23.7 ± 0.2 °C, vapor pressure deficit (VPD) of 1.5 ± 0.2 kPa, and CO_2 concentration of 814.2 ± 28.7 $\mu\text{mol}\cdot\text{mol}^{-1}$ (mean \pm standard deviation).

At 3 weeks after seeding, the plants with 6–8 true leaves were transferred to an experimental growth chamber (E15; Conviron, Winnipeg, Manitoba, Canada) under ambient CO_2 and hand-watered daily with the same nutrient solution. The chamber was equipped with six 200-W white LED bars (Rev-2; GrowRay, Boulder, CO, USA) with 50% red, 20% green, 24% blue, and 6% far-red, mounted 40 cm above the canopy. Spectral distributions were verified using a spectrometer (LI-180; LI-COR Biosciences, Lincoln, NE, USA). The lighting operated from 0:00 to 16:00 (16 h).

2.3 CF measurement

CF was measured on the same uppermost fully expanded leaf throughout the 7-day period to track temporal responses to treatments. A pulse-amplitude modulated (PAM) fluorometer (MINI-PAM; Heinz Walz, Effeltrich, Germany), remotely controlled by a datalogger (CR1000; Campbell Scientific, Logan, UT, USA) via an RS-232 interface, was used for *in situ* measurements in the growth chamber. Through serial communication, the datalogger automatically executed measurement commands, retrieved data, and calculated the fluorescence parameters (Nam et al., 2025).

Every 30 minutes during the 16-h photoperiod, saturating light pulses were applied to determine maximum fluorescence in light (F_m'), with steady-state fluorescence (F_t) measured immediately beforehand. The white LED light was then briefly turned off, and a 2-second pulse of far-red light was applied to measure minimal fluorescence in light (F_o'), after which white light resumed. The operating PSII efficiency (Φ_{PSII}) was calculated as $(F_m' - F_t)/F_m'$ (Genty et al., 1989) to estimate the proportion of absorbed light

used in photochemistry. ETR, representing the overall photosynthetic capacity, was estimated as $\Phi_{\text{PSII}} \times \text{PPFD} \times 0.5 \times 0.84$, assuming an equal distribution of photons between PSI and PSII and an 84% incident light absorption (Maxwell and Johnson, 2000).

Light-adapted maximum quantum efficiency (F_v'/F_m') was calculated as $(F_m' - F_o')/F_m'$, which represents the maximum efficiency of PSII while acclimated at a given light intensity (Baker et al., 2007). Dark-adapted parameters (F_o and F_m) were measured hourly from 16:00 to 0:00, and dark-adapted maximum efficiency of PSII (F_v/F_m) was calculated as $(F_m - F_o)/F_m$. F_v/F_m measured after 1 and 8 hours of dark adaptation (F_v/F_m 1h and F_v/F_m 8h) were used to assess PSII recovery, as photoprotective and photoinhibitory components of non-photochemical quenching (NPQ) relax at different rates, ranging from minutes to several hours, depending on stress severity (Maxwell and Johnson, 2000). Lake model-based photochemical quenching coefficient (qL) represents the fraction of PSII reaction centers that are open. Quantum yield of NPQ (Φ_{NPQ}) and quantum yield of non-regulated energy dissipation (Φ_{NO}) were calculated following Kramer et al. (2004).

Photochemical quenching coefficient (qP) = $(F_m' - F_t)/(F_m' - F_o')$

$$qL = qP \times (F_o' / F_t)$$

$$\text{NPQ} = (F_m - F_m') / F_m'$$

$$\Phi_{\text{NO}} = 1 / (\text{NPQ} + 1 + qL \times ((F_m / F_o) - 1))$$

$$\Phi_{\text{NPQ}} = 1 - \Phi_{\text{PSII}} - \Phi_{\text{NO}}$$

Measurements were taken automatically by the datalogger using a proprietary software (LoggerNet v.4.7; Campbell Scientific, Logan, UT, USA). The datalogger triggered measurements of F_m/F_m' , F_o/F_o' , and F_t every 30 minutes during the photoperiod and hourly during the dark period. These raw fluorescence values were subsequently used to calculate various CF parameters. Additionally, with the integration of far-red LED light into the automated CF measurement protocol, parameters that require F_o' to be calculated, such as F_v'/F_m' and qL, can be obtained throughout the daytime in the presence of ambient light. Cumulative ETR was calculated by integrating instantaneous ETR values measured at 15-min intervals during the photoperiod across the entire experimental period. This metric quantifies the total photochemical electron flux processed by PSII over time and was used to evaluate the relationship between integrated photochemical activity and final shoot biomass.

2.4 Leaf photosynthesis measurements and harvest

Leaf gas exchange was measured on the uppermost fully expanded leaves at two days after treatment (DAT) and DAT 7 using a portable photosynthesis system (CIRAS-3; PP Systems,

Amesbury, MA, USA). Net photosynthetic rate (A), stomatal conductance (g_s), transpiration rate (E), intercellular CO_2 concentration (C_i), and water use efficiency (WUE) were recorded under a constant CO_2 concentration of $400 \mu\text{mol}\cdot\text{mol}^{-1}$, reflecting typical ambient CO_2 levels for standardized measurements.

At DAT 7, rapid $A-C_i$ response curves were obtained using a high-speed CO_2 ramping technique (Stinziano et al., 2017) to assess photosynthetic capacity and identify limiting factors under experimental stress conditions. CO_2 concentration was ramped from 100 to $1500 \mu\text{mol}\cdot\text{mol}^{-1}$ over 6 minutes, with baseline cuvette response established using an empty cuvette. Post-data processing was conducted to recompute actual A and C_i values using a spreadsheet provided by the portable photosynthesis system. Curve fitting was then performed by minimizing the residual sum of squares, as described by Sharkey et al. (2007), to derive the maximum rate of ribulose-1,5-bisphosphate carboxylase oxygenase (Rubisco) carboxylation ($V_{c,\text{max}}$), the maximal rate of electron transport (J_{max}), and triose phosphate utilization (TPU). More details regarding the methodology of the rapid A/C_i curves can be found in PPSystems (2022) and Liu and van Iersel (2021).

While gas exchange parameters at DAT 2 were directly measured under a steady CO_2 concentration, those at DAT 7 were extracted from the ramping data point at $400 \mu\text{mol}\cdot\text{mol}^{-1}$ CO_2 . During all gas exchange measurements, environmental conditions in the cuvette (temperature, light intensity, and humidity) were set to match the corresponding experimental conditions. Measurements were conducted between 14:00 and 16:00 to minimize the effect of the time of day.

All lettuce plants were harvested at DAT 7. Shoot fresh weight was measured immediately, and shoot dry weight was determined after oven-drying at 80°C for 72 hours. Shoot water content was measured to evaluate stress-induced dehydration and morphological adaptation, and it was calculated as (shoot fresh weight – shoot dry weight)/shoot fresh weight. Leaf chlorophyll content was measured using a handheld chlorophyll meter (CCM-220 plus; Opti-Sciences, Hudson, NH, USA) on six uppermost fully expanded leaves per plant, and the values were averaged.

2.5 Treatments and experimental design

Plants were exposed to three temperatures (18, 25, and 32°C) and two light intensities (150 and $500 \mu\text{mol}\cdot\text{m}^{-2}\cdot\text{s}^{-1}$ PPF) for 7 days. The temperature treatments were selected to span a physiologically relevant range for lettuce, with 25°C representing near-optimal daytime conditions and 18 and 32°C representing cooler and warmer conditions that may induce stress (Holmes et al., 2019; Zhou et al., 2022). The two PPF levels, applied under a 16-h photoperiod, corresponded to DLI of 8.64 and $28.8 \text{ mol}\cdot\text{m}^{-2}\cdot\text{d}^{-1}$, representing typical greenhouse light conditions, within ranges where lettuce growth increases with PPF and DLI (Faust and Logan, 2018; Mayorga-Gomez et al., 2024).

The actual average temperatures and light levels recorded across all replicates during the treatment period were 18.1 ± 1.0 , 24.8 ± 0.3 , and $31.9 \pm 0.4^\circ\text{C}$, and 150.0 ± 0.6 and $500.7 \pm 2.7 \mu\text{mol}\cdot\text{m}^{-2}\cdot\text{s}^{-1}$,

respectively. Light intensity was continuously monitored using photodiodes (SLD-69C1; Silonex, Montreal, Quebec, Canada), with one sensor placed at canopy height per experimental unit. All photodiodes were calibrated against a quantum sensor (MQ-500; Apogee Instruments, Logan, UT, USA) before the experiment and connected to a datalogger for real-time monitoring and light adjustment.

The average VPD was 0.99 ± 0.16 , 1.20 ± 0.18 , and 1.21 ± 0.22 kPa, and the corresponding relative humidity (RH) values were $52.7\% \pm 5.4\%$, $61.6\% \pm 5.7\%$, and $74.5\% \pm 4.4\%$ at 18, 25, and 32°C , respectively. In the growth chamber, humidity was controlled to balance VPD among temperature treatments. At 32°C , humidifiers (Classic 300S Ultrasonic Smart Humidifier; Levoit, Anaheim, CA, USA) were used to maintain approximately 75% RH, whereas at 18°C , two dehumidifiers (800 sq ft dehumidifier; Gocheer, Shenzhen, China) operated at full capacity to reduce RH and increase VPD, although values above ~ 1.2 kPa could not be achieved.

The experiment was arranged as a split-plot randomized complete block design (RCBD) conducted over 12 weeks in a single growth chamber. Due to spatial limitations, blocks were arranged temporally, with each 3-week period considered one block and the sequence repeated four times, resulting in a total of 12 weeks. Temperature (whole-plot factor) was randomly assigned weekly to each experimental unit (7-day period) within each block ($n = 4$). A reflective partition divided the chamber into two sections (left and right) for the light treatments (split-plot factor), with 150 and $500 \mu\text{mol}\cdot\text{m}^{-2}\cdot\text{s}^{-1}$ PPF applied at each light intensity randomly within each temperature condition. The temperature was uniform across the chamber during the experimental period.

2.6 Statistical analysis

All statistical analyses were conducted in statistical software (R version 4.5.0; R Foundation for Statistical Computing, Vienna, Austria). Linear mixed-effects models were used for all analyses, with experimental block included as a random effect. For CF parameters, three-way analysis of variance (ANOVA) was performed with temperature, PPF, and DAT as fixed factors. The fixed-effects structure of the model was $y_{ijkl} = \mu + T_i + P_j + D_k + (TP)_{ij} + (TD)_{ik} + (PD)_{jk} + (TPD)_{ijk} + b_l + \epsilon_{ijkl}$, where T , P , and D represent the effects of temperature, PPF, and DAT effect, respectively, b_l represents the random effect of experimental block, and ϵ_{ijkl} is the residual error. Because CF parameters were measured repeatedly over time, a continuous autoregressive correlation structure (corCAR1) was used to account for temporal autocorrelation among observations. Variance weighting was also applied to address heteroscedasticity observed across temperature and PPF treatments. Model structures were evaluated sequentially, and autocorrelation functions (ACF) of normalized residuals were used to confirm that temporal autocorrelation was adequately accounted for without introducing unnecessary model complexity. For gas exchange, A/C_i curve, and harvest parameters, two-way ANOVA was conducted with temperature and PPF as

fixed factors. Pairwise comparisons were performed using Tukey's Honestly Significant Difference (HSD) test at a 95% confidence level. For the correlation between ETR and A , linear models were constructed that included interaction terms of ETR with temperature, DAT, and the interaction of temperature \times DAT to test how these factors influenced the slope of the A -ETR relationship. Model assumptions were evaluated using residual diagnosis, including residual-fitted plots and quantile-quantile plots, to confirm homoscedasticity and normality of residuals.

3 Results

3.1 Real-time monitoring of photochemical activities

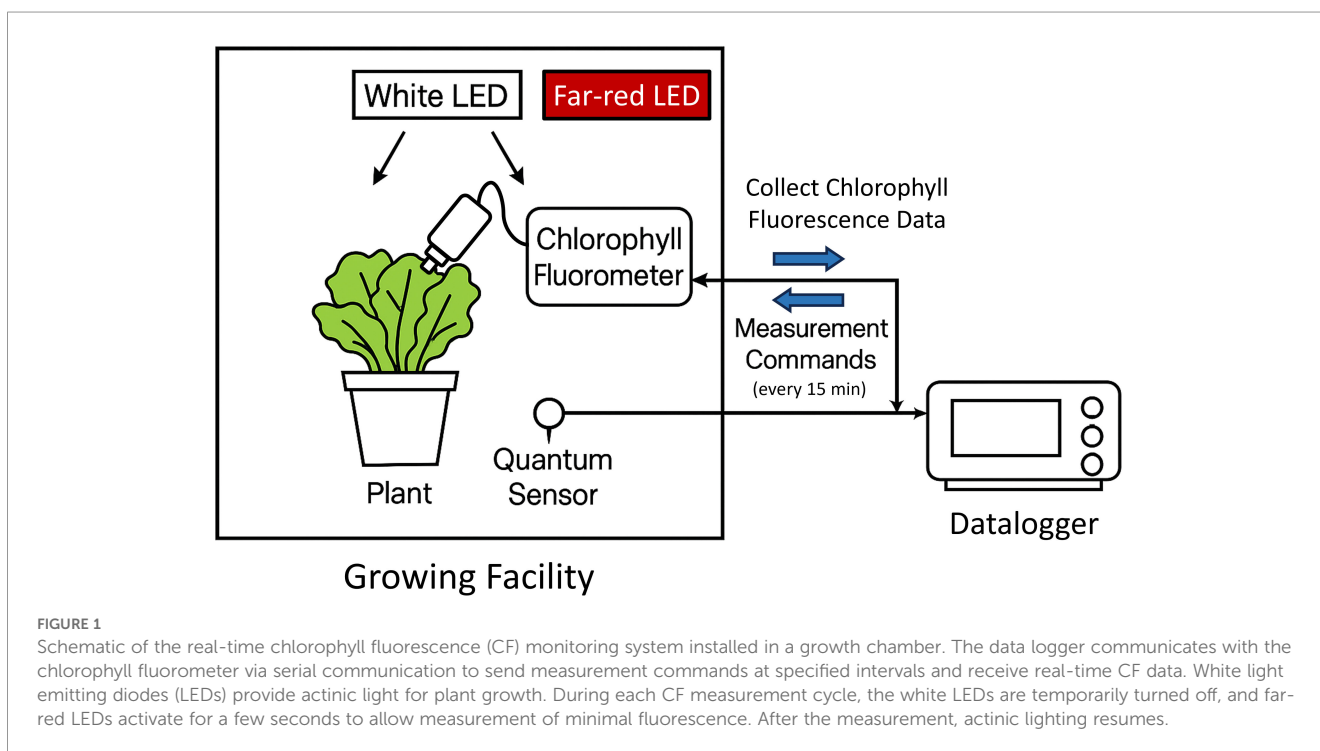
A real-time CF monitoring system (Figure 1) was used to collect high-temporal-resolution data on photochemical activity every 30 minutes during the photoperiod and every hour at night. This setup enabled continuous monitoring of CF over a 7-day period, capturing both daily and within-day changes under different temperature and light conditions (Figure 2). Φ_{PSII} gradually increased during the daytime within each day, particularly under 32°C with low light and under high light (500 $\mu\text{mol}\cdot\text{m}^{-2}\cdot\text{s}^{-1}$ PPFD) across all temperatures, suggesting short-term photochemical adjustments to heat and light stress (Figures 2A, B). These diurnal changes were associated with a diurnal decrease in Φ_{NPQ} and Φ_{NO} , reflecting a shift in energy distribution from non-photochemical to photochemical processes (Figures 2E-H). Notably, a distinct zigzag pattern in Φ_{PSII} was observed under 32°C and 150 $\mu\text{mol}\cdot\text{m}^{-2}\cdot\text{s}^{-1}$ PPFD, characterized by a daytime increase followed by an abrupt decrease the next morning,

leading to an overall decline from DAT 2 to 7. In contrast, plants under 500 $\mu\text{mol}\cdot\text{m}^{-2}\cdot\text{s}^{-1}$ PPFD showed a more continuous increase in Φ_{PSII} , with minimal discrepancies between days.

3.2 Photosynthetic efficiency and energy dissipation

Overall, Φ_{PSII} was lower under 500 $\mu\text{mol}\cdot\text{m}^{-2}\cdot\text{s}^{-1}$ than under 150 $\mu\text{mol}\cdot\text{m}^{-2}\cdot\text{s}^{-1}$, and there was no temperature effect alone (Table 1), but the temperature effect varied depending on PPFD (Figures 2A, B). At 150 $\mu\text{mol}\cdot\text{m}^{-2}\cdot\text{s}^{-1}$, Φ_{PSII} was lowest at 32°C, whereas at 500 $\mu\text{mol}\cdot\text{m}^{-2}\cdot\text{s}^{-1}$, it was lowest at 18°C. Across all conditions, 25°C consistently showed the highest Φ_{PSII} , indicating that specific combinations of light intensity and temperature could be suboptimal for maintaining photochemical efficiency in lettuce. Although Φ_{PSII} tended to decrease at extreme temperatures, these differences were not statistically significant when averaged across time (Figure 3A).

Daily means of CF values were calculated to assess the effects of temperature, light intensity, and DAT, as the 30-minute interval data showed high autocorrelation and were difficult to analyze directly (Figure 4). Φ_{PSII} was also affected by DAT, with trends depending on both temperature and PPFD. At 25 and 32°C, Φ_{PSII} remained relatively constant over time, while values at 18°C increased by approximately 10%, suggesting a recovery response (Figure 4A). Under 500 $\mu\text{mol}\cdot\text{m}^{-2}\cdot\text{s}^{-1}$ PPFD, Φ_{PSII} gradually increased by about 14% over the 7-day period, while under 150 $\mu\text{mol}\cdot\text{m}^{-2}\cdot\text{s}^{-1}$, it decreased slightly by less than 4% (Figure 4B). Initially, Φ_{PSII} under 150 $\mu\text{mol}\cdot\text{m}^{-2}\cdot\text{s}^{-1}$ was 24% higher than under 500 $\mu\text{mol}\cdot\text{m}^{-2}\cdot\text{s}^{-1}$, but the difference narrowed to only 5% by the end of the experiment. This suggests that plants showed the most pronounced acclimation over time in photosynthetic efficiency under high light and low temperature.



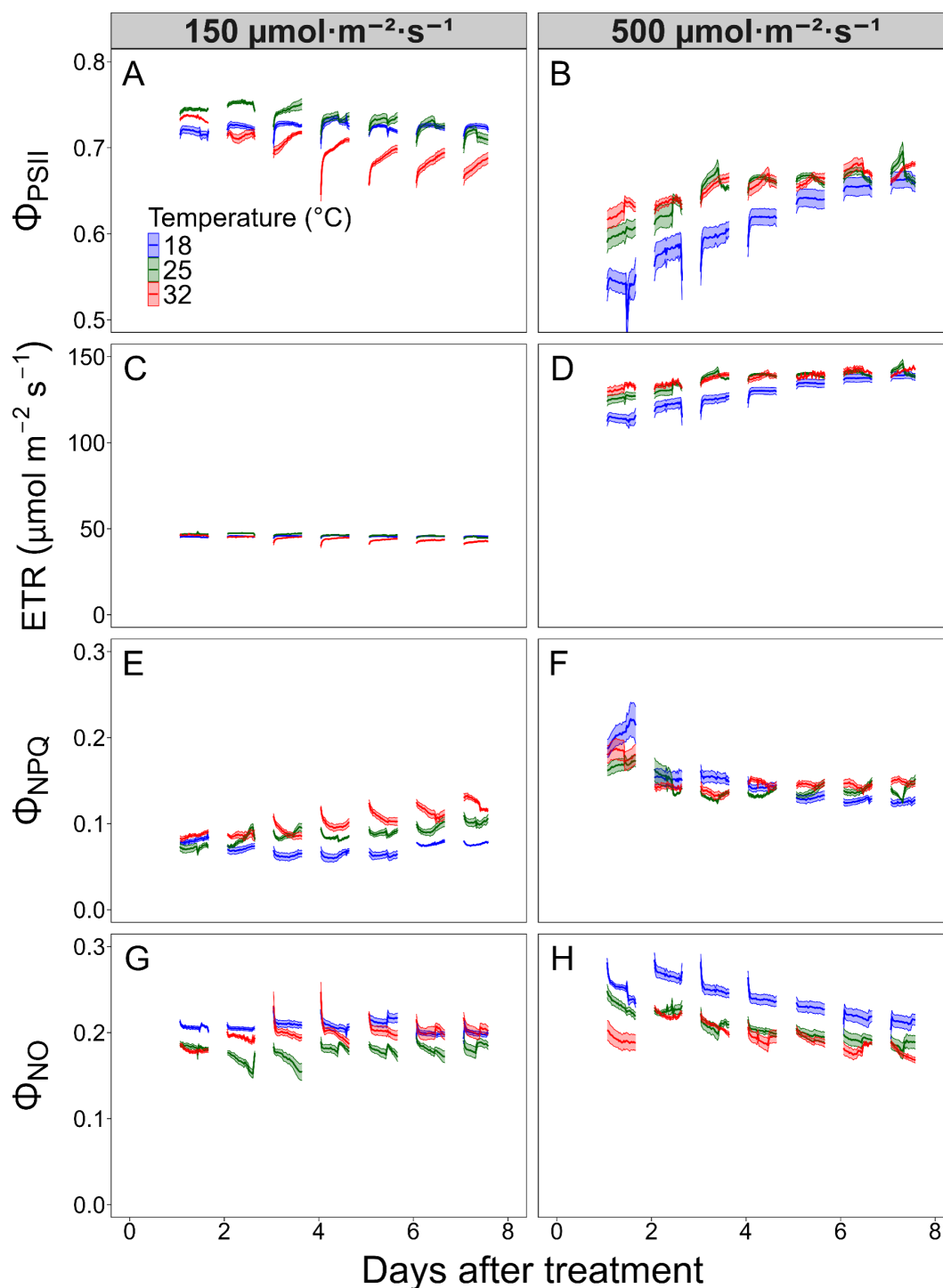


FIGURE 2
Chlorophyll fluorescence parameters were measured every 30 minutes during a 16-hour photoperiod in lettuce (*Lactuca sativa* ‘Green Towers’) grown under two photosynthetic photon flux densities (PPFD) (150 and 500 $\mu\text{mol}\cdot\text{m}^{-2}\cdot\text{s}^{-1}$) and three temperature conditions (18, 25, and 32 °C) for seven days. Data were collected for the operating photosystem II (PSII) efficiency (Φ_{PSII}) (A, B), electron transport rate (ETR) (C, D), quantum yield of non-photochemical quenching (Φ_{NPQ}) (E, F), and quantum yield of non-regulated energy dissipation (Φ_{NO}) (G, H). Solid lines indicate mean values, and shaded areas indicate standard errors (n = 4). Some standard error areas are not visible due to their minimal size.

ETR was approximately three times higher under 500 $\mu\text{mol}\cdot\text{m}^{-2}\cdot\text{s}^{-1}$ compared to 150 $\mu\text{mol}\cdot\text{m}^{-2}\cdot\text{s}^{-1}$, with average values of approximately 134 and 45 $\mu\text{mol}\cdot\text{m}^{-2}\cdot\text{s}^{-1}$, respectively (Table 1). Compared to Φ_{PSII} , the effects of temperature and DAT on ETR were relatively minor

(Figures 3B, 4C), but followed the same overall pattern of Φ_{PSII} , as ETR is calculated from Φ_{PSII} , incident PPFD, and fixed coefficients.

Φ_{NPQ} and Φ_{NO} represent the proportion of absorbed light dissipated as heat or lost through unregulated pathways rather

TABLE 1 Effects of temperature, photosynthetic photon flux density (PPFD), and days after treatment (DAT) on daily averaged chlorophyll fluorescence parameters; operating photosystem II (PSII) efficiency (Φ_{PSII}), electron transport rate (ETR), quantum yield of non-photochemical quenching (Φ_{NPQ}), quantum yield of non-regulated energy dissipation (Φ_{NO}), light-adapted maximum quantum efficiency (F_v'/F_m'), 1-hour dark-adapted maximum quantum efficiency (F_v/F_m 1h), 8-hour dark-adapted maximum quantum efficiency (F_v/F_m 8h), and photochemical quenching coefficient (qL).

Treatments		Φ_{PSII}	ETR	Φ_{NPQ}	Φ_{NO}	F_v'/F_m'	F_v/F_m 1h	F_v/F_m 8h	qL
Temperature (T)	18 °C	0.670 ± 0.011 a	87.5 ± 2.3 a	0.109 ± 0.006	0.221 ± 0.006 a	0.748 ± 0.003 a	0.753 ± 0.006 b	0.820 ± 0.003 ab	0.707 ± 0.022 b
	25 °C	0.695 ± 0.003 a	91.8 ± 0.8 a	0.114 ± 0.003	0.191 ± 0.005 b	0.740 ± 0.003 a	0.776 ± 0.003 a	0.831 ± 0.001 a	0.806 ± 0.031 ab
	32 °C	0.680 ± 0.005 a	91.3 ± 0.8 a	0.124 ± 0.004	0.195 ± 0.002 b	0.714 ± 0.003 b	0.757 ± 0.003 ab	0.813 ± 0.002 b	0.869 ± 0.009 a
PPFD (P)	150 $\mu\text{mol}\cdot\text{m}^{-2}\cdot\text{s}^{-1}$	0.722 ± 0.002 a	45.5 ± 0.1 b	0.086 ± 0.003 b	0.193 ± 0.003 b	0.747 ± 0.002 a	0.778 ± 0.003 a	0.820 ± 0.003 a	0.874 ± 0.011 a
	500 $\mu\text{mol}\cdot\text{m}^{-2}\cdot\text{s}^{-1}$	0.642 ± 0.004 b	134.9 ± 0.9 a	0.146 ± 0.003 a	0.212 ± 0.002 a	0.721 ± 0.001 b	0.746 ± 0.002 b	0.823 ± 0.001 a	0.714 ± 0.010 b
P-values									
	T	0.025	0.019	0.61	0.028	0.014	< 0.001	0.0078	0.016
	P	< 0.001	< 0.001	< 0.001	< 0.001	< 0.001	< 0.001	0.0054	< 0.001
	DAT	0.49	0.50	0.78	0.33	0.94	0.76	0.013	0.26
	T × P	0.037	0.0013	0.29	0.30	0.034	0.17	0.070	0.75
	T × DAT	< 0.001	< 0.001	0.0037	0.13	< 0.001	< 0.001	0.010	0.97
	P × DAT	< 0.001	< 0.001	< 0.001	0.0076	< 0.001	< 0.001	< 0.001	< 0.001
	T × P × DAT	0.88	0.079	0.74	0.83	0.67	0.58	0.95	0.60

Values are means ± standard error (n = 4), and different letters within a column from the same factor indicate significant differences at $\alpha = 0.05$, according to Tukey's Honestly Significant Difference (HSD) test.

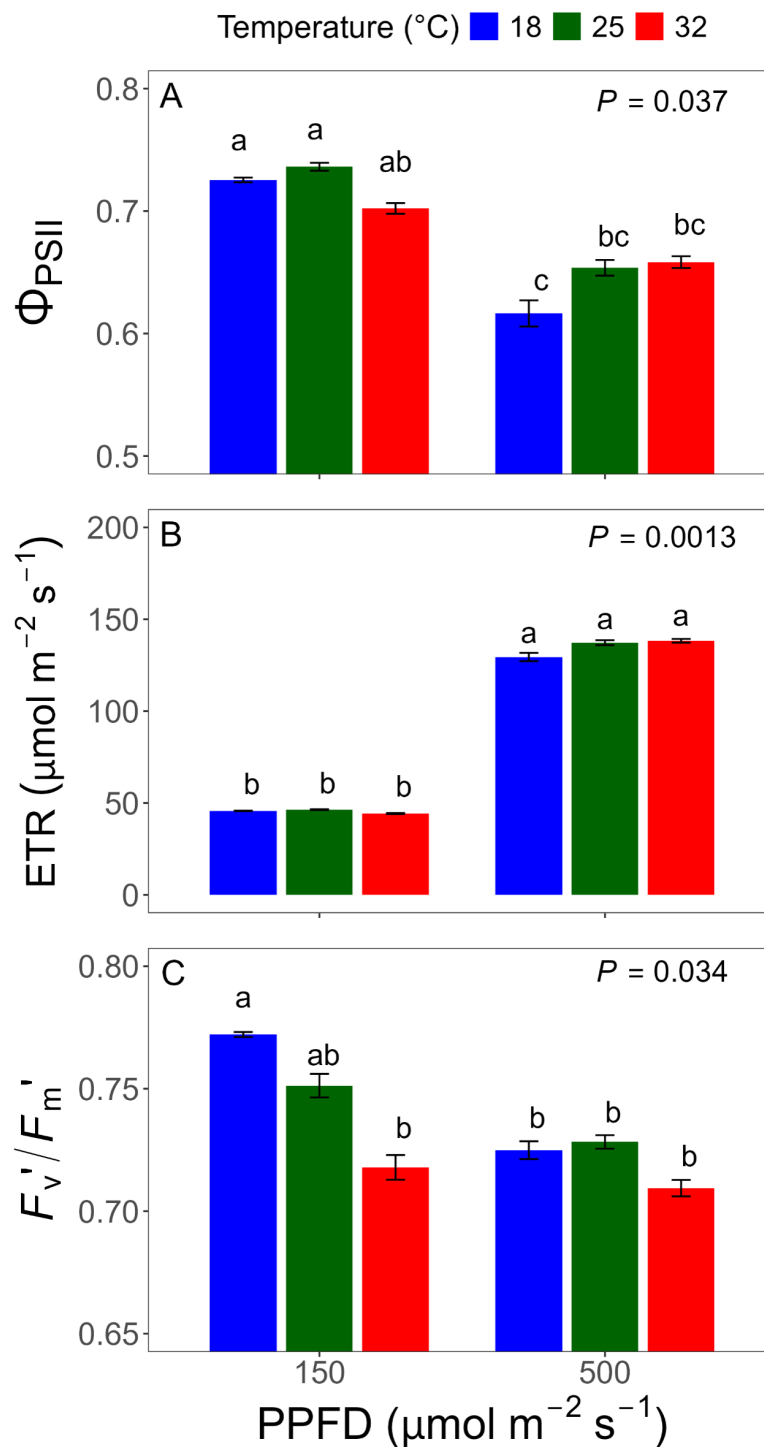


FIGURE 3
 Chlorophyll fluorescence parameters for temperature x photosynthetic photon flux density (PPFD) interactions were statistically significant. Data represent means of operating photosystem II (PSII) efficiency (Φ_{PSII}) (A), electron transport rate (ETR) (B), and light-adapted maximum quantum efficiency (F_v'/F_m') (C), averaged across days after treatment. Different letters indicate significant differences ($P < 0.05$) based on Tukey's Honestly Significant Difference (HSD) test. Error bars represent standard errors (n = 4).

than being used for photochemistry. Both parameters were significantly higher under 500 $\mu\text{mol m}^{-2} \text{s}^{-1}$ compared to 150 $\mu\text{mol m}^{-2} \text{s}^{-1}$, indicating that higher light intensity increased non-photochemical energy dissipation, which was associated with reduced photosynthetic efficiency (Figures 4F, H).

Over time, Φ_{NPQ} and Φ_{NO} decreased under 500 $\mu\text{mol m}^{-2} \text{s}^{-1}$, corresponding with a gradual increase in Φ_{PSII} , suggesting acclimation to high light. In contrast, under 150 $\mu\text{mol m}^{-2} \text{s}^{-1}$, Φ_{NPQ} and Φ_{NO} remained stable, resulting in stable Φ_{PSII} . Temporal trends differed between the two parameters. Under 500

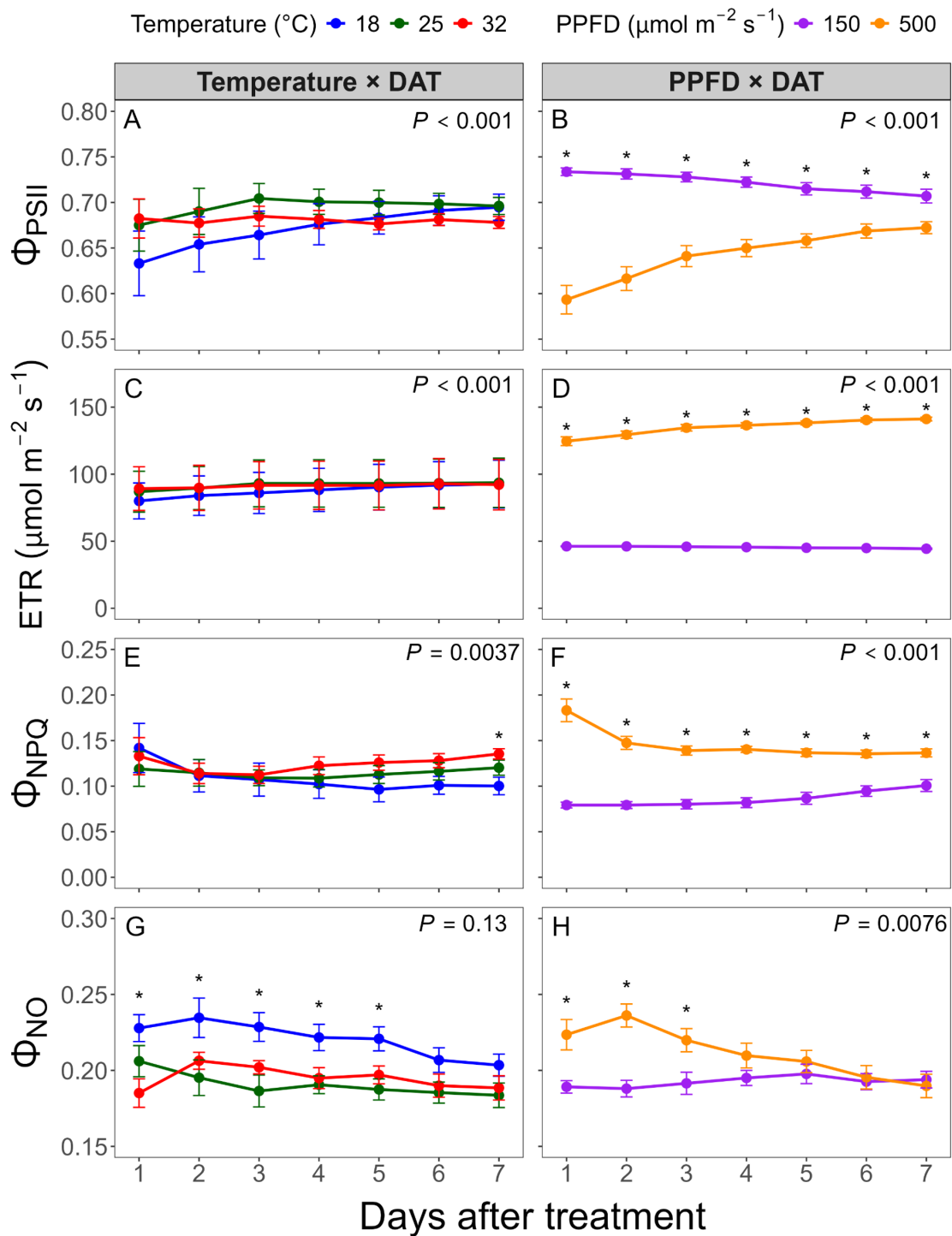


FIGURE 4

Daily mean values of chlorophyll fluorescence parameters measured over seven days after treatment (DAT). Parameters include operating photosystem II (PSII) efficiency (Φ_{PSII}) (A, B), electron transport rate (ETR) (C, D), quantum yield of non-photochemical quenching (Φ_{NPQ}) (E, F), and quantum yield of non-regulated energy dissipation (Φ_{NO}) (G, H). Left panels (A, C, E, G) show temperature × DAT interactions averaged across photosynthetic photon flux density (PPFD) levels; right panels (B, D, F, H) show PPFD × DAT interactions averaged across temperature levels. Asterisks indicate significant differences between treatments at each time point ($P < 0.05$). Error bars represent standard errors ($n = 4$).

$\mu\text{mol}\cdot\text{m}^{-2}\cdot\text{s}^{-1}$, Φ_{NPQ} exhibited a significant decrease during the first day and remained stable thereafter (Figure 4F), while Φ_{NO} gradually decreased throughout the experiment (Figure 4H). As a result, by the end of the 7-day period, there was no significant difference in Φ_{NO}

between the two light conditions. Temperature effects on Φ_{NPQ} over time were not clearly distinct, but at the end of the experiment, Φ_{NPQ} was highest at 32°C, followed by 25 and 18°C (Figure 4E). In contrast, Φ_{NO} remained highest at 18°C throughout most of the

experiment period, though differences among temperatures were no longer significant by DAT 6 and 7.

3.3 Temporal changes in maximum quantum efficiency

Daily mean values of F_v'/F_m' , an estimate of maximum quantum efficiency at a given light intensity if all PSII centers were open, showed a different trend compared to Φ_{PSII} . F_v'/F_m' was higher under 150 than 500 $\mu\text{mol}\cdot\text{m}^{-2}\cdot\text{s}^{-1}$, but gradually decreased over time, whereas it remained relatively stable under 500 $\mu\text{mol}\cdot\text{m}^{-2}\cdot\text{s}^{-1}$ (Figure 5B). Temperature effects were also observed: F_v'/F_m' was highest at 18°C, followed by 25 and 32°C under 150 $\mu\text{mol}\cdot\text{m}^{-2}\cdot\text{s}^{-1}$ (Figure 3C), with increasing values at 18 °C and decreasing trends at 25 and 32°C (Figure 5A).

The average F_v/F_m across all treatments and DAT was 0.762 after 1 hour of dark adaptation, but stabilized at 0.821 from 2 through 8 hours after dark adaptation, indicating that full recovery was reached within the initial two hours. Therefore, F_v/F_m 1h and F_v/F_m 8h were selected to assess transient and sustained effects of environmental stress. Under 150 $\mu\text{mol}\cdot\text{m}^{-2}\cdot\text{s}^{-1}$, F_v/F_m decreased over time, while it increased under 500 $\mu\text{mol}\cdot\text{m}^{-2}\cdot\text{s}^{-1}$ (Figures 5D, F). F_v/F_m 1h was consistently higher under 150 $\mu\text{mol}\cdot\text{m}^{-2}\cdot\text{s}^{-1}$, but F_v/F_m 8h under 500 $\mu\text{mol}\cdot\text{m}^{-2}\cdot\text{s}^{-1}$ recovered fully, approaching 0.83, the commonly accepted optimal value. F_v/F_m 1h and F_v/F_m 8h were highest at 25°C and lower under suboptimal temperatures (Figures 5C, E). However, F_v/F_m 8h at 18°C recovered to approximately 0.83 by DAT 6 and 7, while values at 32°C remained low around 0.813, suggesting more persistent stress at higher temperatures despite a sufficient dark adaptation period.

qL, the proportion of open PSII reaction centers, also showed clear temperature and light effects. qL was highest at 32°C, followed by 25 and 18°C, and these temperature-dependent differences remained nearly constant throughout the experiment (Figure 5G). Under 150 $\mu\text{mol}\cdot\text{m}^{-2}\cdot\text{s}^{-1}$, qL remained stable, whereas it gradually increased under 500 $\mu\text{mol}\cdot\text{m}^{-2}\cdot\text{s}^{-1}$ (Figure 5H). Consequently, the large initial difference between light intensities diminished by DAT 3.

3.4 Leaf gas exchange parameters

Leaf gas exchange measurements were conducted to examine whether the effects of temperature and light intensity observed in CF were also reflected in CO₂ assimilation and stomatal responses. Measurements were taken on DAT 2 and 7 to capture both early stress responses and potential acclimation (Figure 6). The *A* was consistently higher at 500 than under 150 $\mu\text{mol}\cdot\text{m}^{-2}\cdot\text{s}^{-1}$ at both time points, regardless of temperature (Figures 6A, B). However, temperature effects varied depending on light intensity and time. Under 150 $\mu\text{mol}\cdot\text{m}^{-2}\cdot\text{s}^{-1}$, temperature differences were minimal. In contrast, under 500 $\mu\text{mol}\cdot\text{m}^{-2}\cdot\text{s}^{-1}$, *A* was lowest at 32°C on DAT 2 but became highest on DAT 7, indicating recovery or acclimation at high temperature.

g_s increased with temperature on DAT 2, with no significant effect of PPFD (Table 2). By DAT 7, under 32°C and 500 $\mu\text{mol}\cdot\text{m}^{-2}\cdot\text{s}^{-1}$, the *g_s* increased by 900 $\text{mmol}\cdot\text{H}_2\text{O}\cdot\text{m}^{-2}\cdot\text{s}^{-1}$ and was 5.6 times higher than in other treatment combinations (Figure 6F). These results indicate strong stomatal adjustment under combined high temperature and high light over time. *E* followed a similar pattern to *g_s*, increasing with temperature across both DATs and PPFD levels. In particular, at DAT 7 under 500 $\mu\text{mol}\cdot\text{m}^{-2}\cdot\text{s}^{-1}$, the *E* was 5.3 times higher at 32°C compared to the lower temperatures (Figure 6G). On both DAT 2 and 7, *C_i* was lower under 500 than under 150 $\mu\text{mol}\cdot\text{m}^{-2}\cdot\text{s}^{-1}$, and 32 °C had the highest *C_i* across temperature treatments (Figure 6E). The overall mean *C_i* decreased from 314 to 231 $\mu\text{mol}\cdot\text{mol}^{-1}$ from DAT 2 to DAT 7. WUE declined with increasing temperature on both dates, with consistently higher values under 500 $\mu\text{mol}\cdot\text{m}^{-2}\cdot\text{s}^{-1}$. The temperature effect on WUE was more pronounced under high light, while differences under 150 $\mu\text{mol}\cdot\text{m}^{-2}\cdot\text{s}^{-1}$ were not statistically significant (Figures 6C, D) ($P > 0.05$).

The relationship between ETR and *A* was significantly affected by temperature ($P < 0.001$) and the interaction between temperature and DAT ($P < 0.001$), but not by DAT alone ($P = 0.31$). Here, the slope of the ETR-*A* relationship reflects the efficiency with which electrons derived from the photosynthetic electron transport chain are utilized for carbon assimilation (Figure 7). At DAT 2, the slope was lowest at 32°C, indicating reduced CO₂ assimilation per unit of electron transport at high temperature. By DAT 7, the slope at 32°C increased and exceeded those at 18 and 25°C, while the slopes at 18 and 25°C decreased over time. These results suggest that the coupling between electron transport and CO₂ fixation was initially suppressed at high temperature but improved with acclimation.

A/C_i response curves were used to illustrate photosynthetic responses across treatments (Supplementary Figure 1). Overall, 500 $\mu\text{mol}\cdot\text{m}^{-2}\cdot\text{s}^{-1}$ resulted in greater *A* values across the *C_i* range. Temperature had no significant main effect on *A*, but a significant interaction between temperature and light intensity was observed ($P = 0.019$), with reduced *A* at 32°C under low light and at 18°C under high light. *V_{c,max}*, *J*, and TPU were estimated from the *A/C_i* curves (Table 3). *V_{c,max}* was 3.8 times higher under 500 than 150 $\mu\text{mol}\cdot\text{m}^{-2}\cdot\text{s}^{-1}$, but the temperature effect varied depending on light intensity (Figure 8). Under 500 $\mu\text{mol}\cdot\text{m}^{-2}\cdot\text{s}^{-1}$, *V_{c,max}* increased with temperature and reached its highest value at 32°C. However, under 150 $\mu\text{mol}\cdot\text{m}^{-2}\cdot\text{s}^{-1}$, *V_{c,max}* remained low across all temperatures *J* was strongly correlated with ETR ($R^2 = 0.92$) and primarily influenced by light intensity, showing higher *J* under higher PPFD without significant temperature effects (Table 3). TPU also increased 2.9 times in response to high light intensity ($P < 0.001$), and a significant interaction was observed. TPU increased with temperature only under 500 $\mu\text{mol}\cdot\text{m}^{-2}\cdot\text{s}^{-1}$ ($P < 0.001$).

3.5 Growth responses

Shoot biomass was highest at 25 °C and under 500 $\mu\text{mol}\cdot\text{m}^{-2}\cdot\text{s}^{-1}$, with shoot dry weight reduced by 28% and 20% at 18°C and 32°C

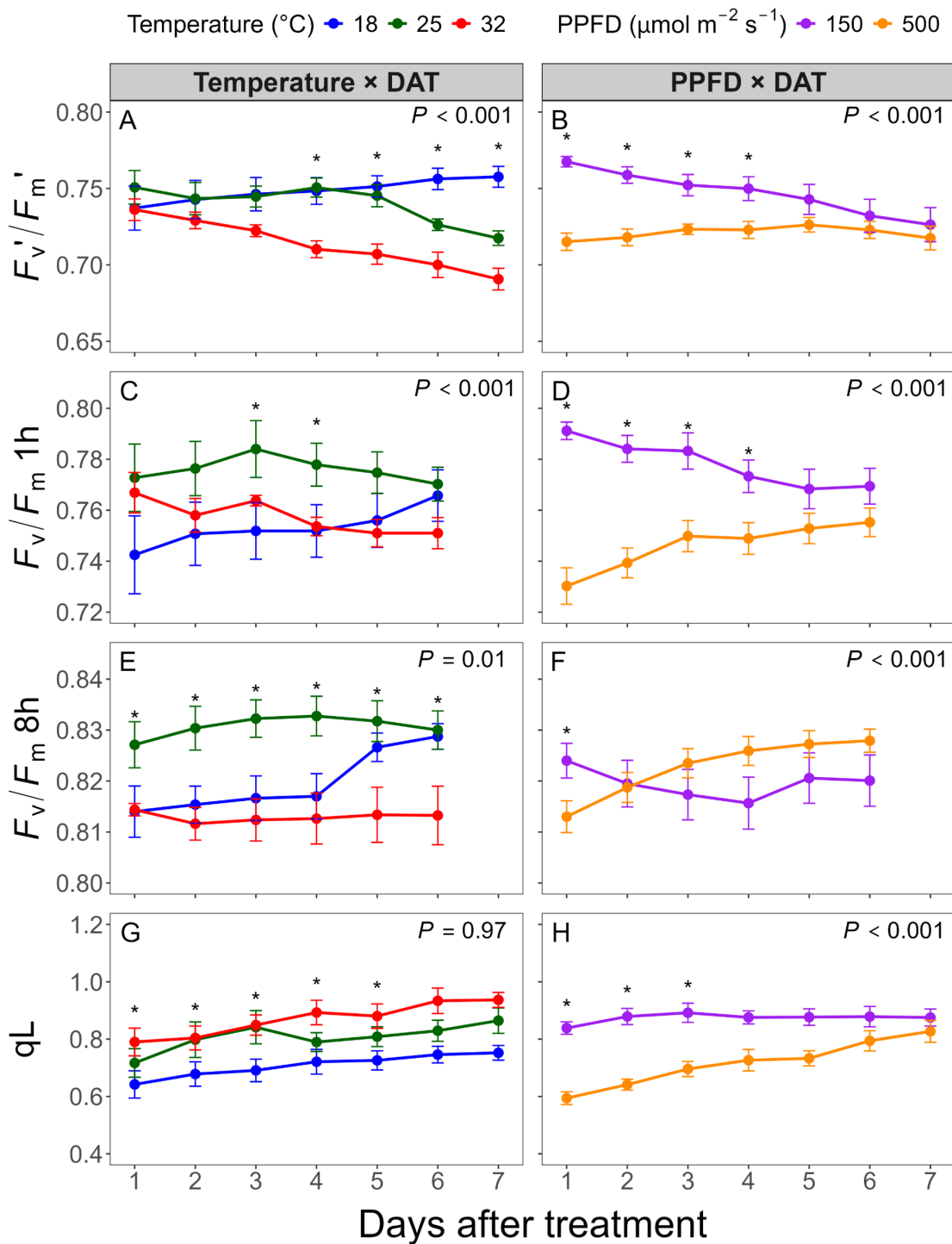


FIGURE 5
 Daily mean values of chlorophyll fluorescence parameters measured over seven days after treatment (DAT). Parameters include light-adapted maximum quantum efficiency (F_v'/F_m') (A, B), 1-hour dark-adapted F_v/F_m (F_v/F_m 1h) (C, D), 8-hour dark-adapted F_v/F_m (F_v/F_m 8h) (E, F), and photochemical quenching coefficient (qL) (G, H). Left panels (A, C, E, G) show temperature \times DAT interactions averaged across photosynthetic photon flux density (PPFD) levels; right panels (B, D, F, H) show PPFD \times DAT interactions averaged across temperature levels. Asterisks indicate significant differences between treatments at each time point ($P < 0.05$). Error bars represent standard errors ($n = 4$).

compared to 25°C (Table 4). Shoot dry weight increased significantly with increasing cumulative ETR ($P < 0.001$; Figure 9). After accounting for cumulative ETR, temperature did not have a significant additional effect on shoot dry weight

($P = 0.592$), and the relationship between cumulative ETR and shoot dry weight did not differ among temperature treatments ($P = 0.342$). Although shoot fresh weight decreased by only 18% under 150 $\mu\text{mol}\cdot\text{m}^{-2}\cdot\text{s}^{-1}$, shoot dry weight decreased by 40%. This

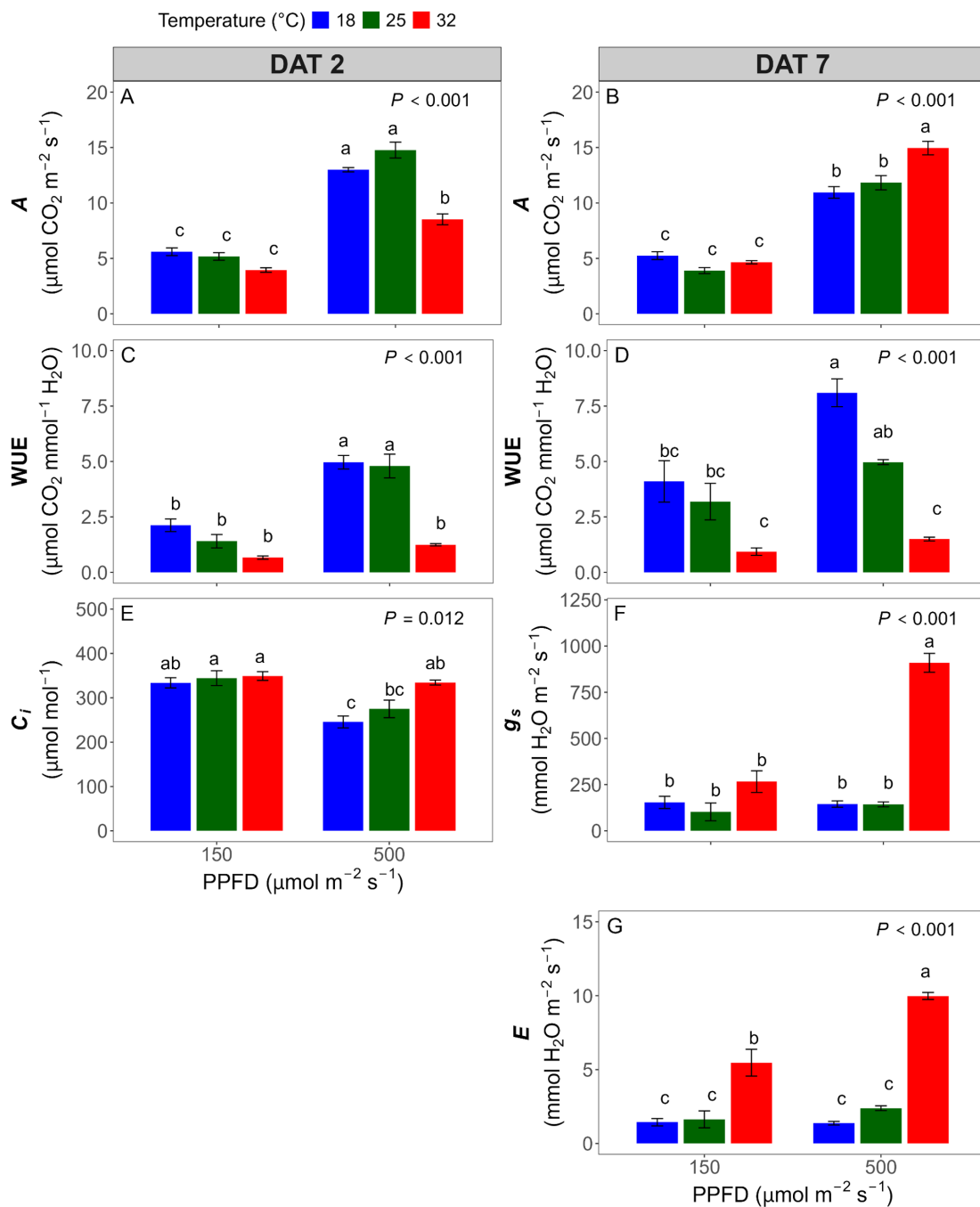


FIGURE 6
 Leaf gas exchange parameters measured at two days (A, C, E) and seven days (B, D, F, G) after treatment. Shown are parameters for which temperature \times photosynthetic photon flux density (PPFD) interactions were statistically significant: photosynthetic rate (A) (A, B), water use efficiency (WUE) (C, D), intercellular carbon dioxide (CO_2) concentration (C_i) (E), stomatal conductance (g_s) (F), and transpiration rate (E) (G). Different letters denote significant differences based on Tukey's Honestly Significant Difference (HSD) test. ($P < 0.05$). Error bars represent standard error ($n = 4$).

discrepancy may be explained by higher shoot water content under low light. Likewise, shoot water content was also highest at the favorable temperature, 25°C. Chlorophyll content was slightly higher under 500 $\mu\text{mol}\cdot\text{m}^{-2}\cdot\text{s}^{-1}$, with no significant effect of temperature. Although temperature \times light intensity interactions were significant for both chlorophyll content and shoot water content, the magnitudes were minimal (Supplementary Figure 2).

4 Discussion

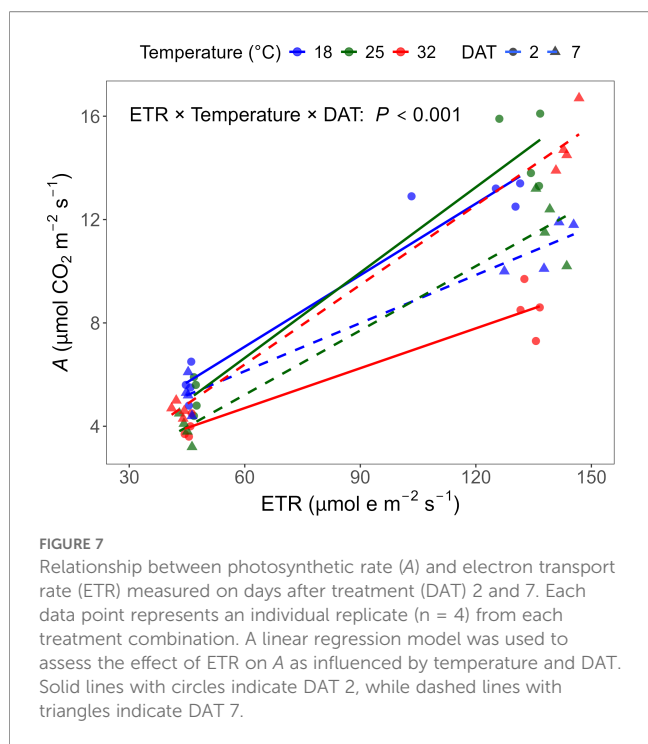
4.1 Light intensity effect on photochemistry

Although photosynthesis increases with light intensity, the photosynthetic efficiency often declines under high light due to

TABLE 2 Effects of temperature and photosynthetic photon flux density (PPFD) on leaf photosynthesis parameters; Photosynthetic rate (A), stomatal conductance (g_s), transpiration rate (E), intercellular carbon dioxide (CO_2) concentration (C_i), and water use efficiency (WUE). Measurements were taken on days after treatment (DAT) 2 and 7, and the data were analyzed separately for each day.

DAT	Treatments		A ($\mu\text{mol}\cdot\text{CO}_2\cdot\text{m}^{-2}\cdot\text{s}^{-1}$)	g_s ($\text{mol}\cdot\text{H}_2\text{O}\cdot\text{m}^{-2}\cdot\text{s}^{-1}$)	E ($\text{mmol}\cdot\text{H}_2\text{O}\cdot\text{m}^{-2}\cdot\text{s}^{-1}$)	C_i ($\mu\text{mol}\cdot\text{mol}^{-1}$)	WUE ($\mu\text{mol}\cdot\text{CO}_2\cdot\text{mmol}^{-1}\cdot\text{H}_2\text{O}$)	
DAT 2	Temperature (T)	18 °C	9.30 ± 0.22 a	145 ± 6 b	2.72 ± 0.20 b	290 ± 6 b	3.55 ± 0.16 a	
		25 °C	9.98 ± 0.42 a	301 ± 40 ab	3.64 ± 0.20 b	310 ± 15 ab	3.10 ± 0.12 a	
		32 °C	6.24 ± 0.21 b	393 ± 58 a	6.54 ± 0.48 a	342 ± 7 a	0.95 ± 0.06 b	
	PPFD (P)	150 $\mu\text{mol}\cdot\text{m}^{-2}\cdot\text{s}^{-1}$	4.91 ± 0.16 b	280 ± 41	4.34 ± 0.24	342 ± 11 a	1.40 ± 0.06 b	
		500 $\mu\text{mol}\cdot\text{m}^{-2}\cdot\text{s}^{-1}$	12.10 ± 0.40 a	279 ± 44	4.26 ± 0.27	285 ± 5 b	3.67 ± 0.14 a	
	P-values							
		<i>T</i>	< 0.001	< 0.001	< 0.001	< 0.001	< 0.001	< 0.001
		<i>P</i>	< 0.001	0.99	0.84	< 0.001	< 0.001	< 0.001
		<i>T</i> × <i>P</i>	< 0.001	0.17	0.24	0.012	< 0.001	< 0.001
DAT 7	Temperature (T)	18 °C	8.10 ± 0.40 b	150 ± 21 b	1.41 ± 0.16 b	223 ± 12 b	6.10 ± 0.73 a	
		25 °C	7.86 ± 0.24 b	123 ± 25 b	2.01 ± 0.27 b	194 ± 13 b	4.08 ± 0.40 a	
		32 °C	9.80 ± 0.29 a	588 ± 9 a	7.72 ± 0.38 a	275 ± 5 a	1.22 ± 0.08 b	
	PPFD (P)	150 $\mu\text{mol}\cdot\text{m}^{-2}\cdot\text{s}^{-1}$	4.60 ± 0.19 b	174 ± 18 b	2.85 ± 0.26 b	256 ± 9 a	2.74 ± 0.25 b	
		500 $\mu\text{mol}\cdot\text{m}^{-2}\cdot\text{s}^{-1}$	12.58 ± 0.16 a	399 ± 12 a	4.58 ± 0.11 a	205 ± 4 b	4.86 ± 0.18 a	
	P-values							
		<i>T</i>	< 0.001	< 0.001	< 0.001	< 0.001	< 0.001	< 0.001
		<i>P</i>	< 0.001	< 0.001	< 0.001	< 0.001	< 0.001	< 0.001
		<i>T</i> × <i>P</i>	< 0.001	< 0.001	< 0.001	0.47	< 0.001	< 0.001

Values are means ± standard error (n = 4). For each DAT, different letters within a column from the same factor indicate significant differences at $\alpha = 0.05$, according to Tukey's Honestly Significant Difference (HSD) test.



excess excitation energy that cannot be used for electron transport and carbon fixation. This energy is instead dissipated via non-photochemical pathways, such as regulated heat dissipation (Φ_{NPQ}) and unregulated energy loss (Φ_{NO}). As shown in previous studies (Kramer et al., 2004), Φ_{NPQ} increases proportionally with light intensity, whereas Φ_{NO} remains relatively unchanged, suggesting that Φ_{NPQ} plays a larger role in reducing photosynthetic efficiency under high light. It is consistent with our observation of elevated Φ_{NPQ} but relatively similar Φ_{NO} under high light conditions compared to low light (Table 1).

Over time, both Φ_{NPQ} and Φ_{NO} declined under high light, while Φ_{PSII} increased, indicating dynamic acclimation (Figure 4). NPQ decreased rapidly and stabilized after DAT 2, which may be

attributed to various physiological responses, such as fast adjustment of the NPQ component, energy-dependent quenching (qE), through lumen acidification, PSII subunit S (PsbS) activation, and the xanthophyll cycle (Murchie and Niyogi, 2011; Zuo, 2025). NPQ is a protective mechanism that safely dissipates excess light as heat, preventing photodamage caused by unregulated energy loss. Hence, moderately high NPQ under high light is not necessarily detrimental, although it reduces photosynthetic efficiency.

In contrast, Φ_{NO} continuously declined throughout the week, suggesting that plants systematically adjusted the photosynthetic machinery and improved light use efficiency through processes associated with changes in light harvesting and electron transport capacity, such as reduced light-harvesting complex II (LHCII) antenna size, chloroplast repositioning, and modulation of electron transport enzymes (Murchie and Niyogi, 2011). The sustained increase in Φ_{PSII} after DAT 2 appeared more closely associated with the decline in Φ_{NO} than with changes in NPQ. This highlights that obtaining Φ_{NPQ} and Φ_{NO} data separately provides insights into the different types of mechanisms driving improvements in photosynthetic efficiency.

qL , which reflects both open PSII reaction centers and the redox state of the plastoquinone (PQ) pool, increased over time under high light, paralleling improvements in Φ_{PSII} (Figure 5H). This recovery may result from enhanced PQ biosynthesis, which replenishes the oxidized PQ pool and facilitates electron transport, as previously reported by Yang et al. (2022).

F_v'/F_m' represents the theoretical maximum efficiency of PSII in the light-adapted state and declines further when severe photoinhibition or electron transport limitations occur after NPQ is saturated (Baker et al., 2007). Its stability under high light (Figure 5B) in this study suggests PSII capacity was preserved, likely due to effective NPQ regulation.

Determining accurate F_v'/F_m' requires a sufficient period of dark adaptation, however, 15–30 minutes is commonly used. Residual qI from prolonged stress, the slowly reversible component of NPQ, can persist for several hours (Tietz et al., 2017). Willits and Peet (2001) emphasized that complete dark adaptation is necessary for

TABLE 3 Effects of temperature and photosynthetic photon flux density (PPFD) on maximum rate of carboxylation ($V_{c,max}$), maximum electron transport rate (J), and triose phosphate utilization rate (TPU), measured on DAT 7.

Treatments		$V_{c,max}$ ($\mu\text{mol}\cdot\text{CO}_2\cdot\text{m}^{-2}\cdot\text{s}^{-1}$)	J ($\mu\text{mol}\cdot\text{m}^{-2}\cdot\text{s}^{-1}$)	TPU ($\mu\text{mol}\cdot\text{CO}_2\cdot\text{m}^{-2}\cdot\text{s}^{-1}$)
Temperature (T)	18 °C	86.6 ± 5.3 b	103.8 ± 5.1	4.63 ± 0.21
	25 °C	151.0 ± 13.4 a	103.0 ± 3.1	5.01 ± 0.12
	32 °C	168.1 ± 8.4 a	92.9 ± 4.2	5.14 ± 0.18
PPFD (P)	150 $\mu\text{mol}\cdot\text{m}^{-2}\cdot\text{s}^{-1}$	56.5 ± 5.1 b	51.3 ± 3.2 b	2.53 ± 0.03 b
	500 $\mu\text{mol}\cdot\text{m}^{-2}\cdot\text{s}^{-1}$	214.0 ± 10.9 a	148.5 ± 5.0 a	7.33 ± 0.20 a
P-values				
	T	< 0.001	0.18	0.057
	P	< 0.001	< 0.001	< 0.001
	T × P	< 0.001	0.22	< 0.001

Values are means ± standard error (*n* = 4), and different letters within a column from the same factor indicate significant differences at α = 0.05, according to Tukey's Honestly Significant Difference (HSD) test.

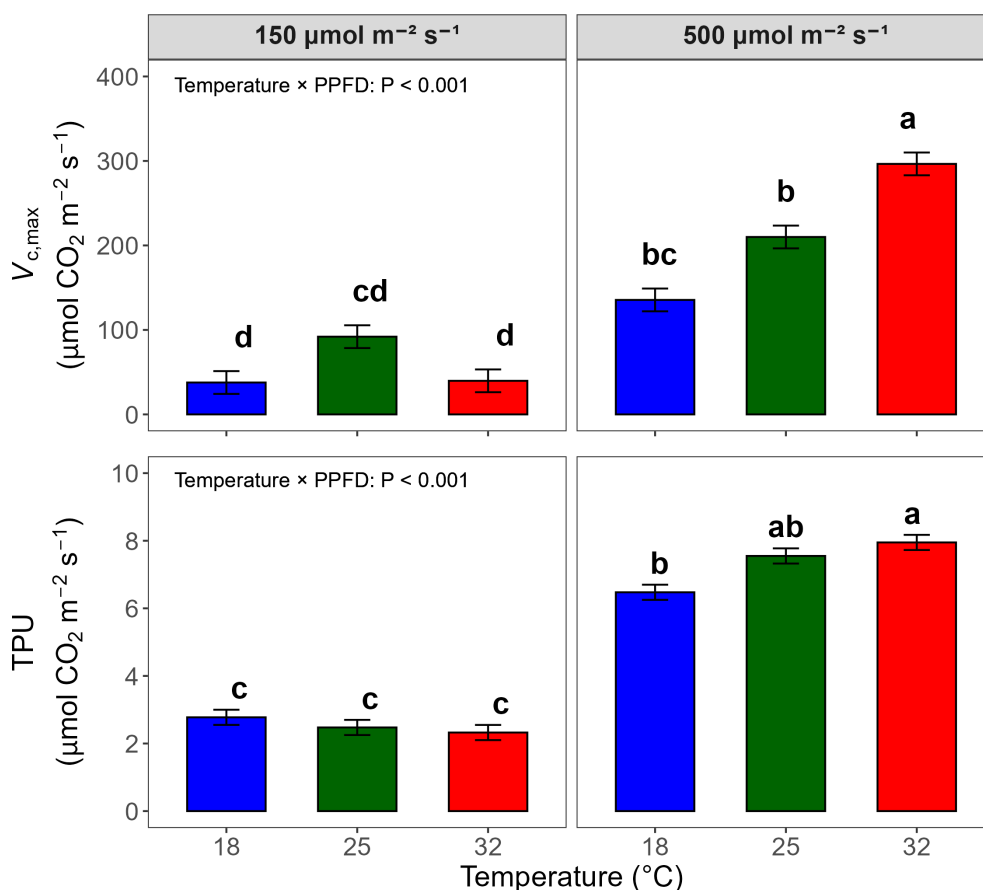
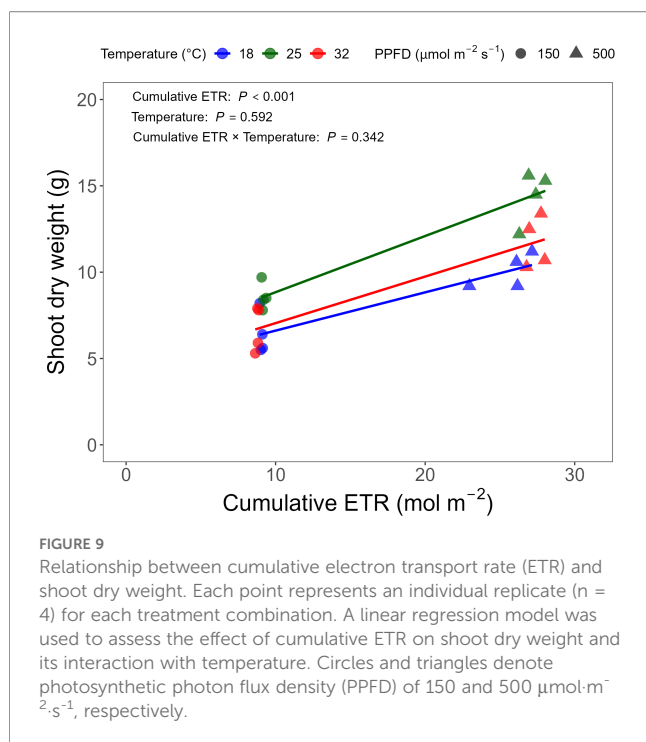


FIGURE 8 Bar graphs of maximum rate of carboxylation ($V_{c,max}$) and triose phosphate utilization rate (TPU) measured on DAT 7, analyzed by two-way analysis of variance (ANOVA) to assess temperature \times photosynthetic photon flux density (PPFD) interactions. Bars represent means ($n = 4$), and different letters indicate significant differences among treatment combinations based on Tukey's Honestly Significant Difference (HSD) test ($P < 0.05$). Error bars represent standard errors.

TABLE 4 Effects of temperature and photosynthetic photon flux density (PPFD) on shoot fresh weight, shoot dry weight, chlorophyll content, and shoot water content, measured at harvest on days after treatment (DAT) 7.

Treatments		Shoot fresh weight (g)	Shoot dry weight (g)	Shoot water content (%)	Chlorophyll content (CCI)
Temperature (T)	18 °C	112.2 ± 8.4 b	8.24 ± 0.56 b	92.7 ± 0.3 b	32.2 ± 0.4
	25 °C	196.2 ± 9.0 a	11.50 ± 0.40 a	94.2 ± 0.2 a	33.2 ± 2.5
	32 °C	134.9 ± 6.3 b	9.23 ± 0.52 b	93.2 ± 0.2 b	30.2 ± 0.7
PPFD (P)	150 μmol·m ⁻² ·s ⁻¹	133.5 ± 6.2 b	7.25 ± 0.32 b	94.5 ± 0.1 a	29.3 ± 1.1 b
	500 μmol·m ⁻² ·s ⁻¹	162.0 ± 4.9 a	12.06 ± 0.34 a	92.3 ± 0.1 b	34.4 ± 0.8 a
P-values					
	T	< 0.001	< 0.001	< 0.001	0.38
	P	0.0014	< 0.001	< 0.001	< 0.001
	T \times P	0.10	0.13	0.031	0.012

Values are means \pm standard error ($n = 4$), and different letters within a column from the same factor indicate significant differences at $\alpha = 0.05$, according to Tukey's Honestly Significant Difference (HSD) test.



the full oxidation of electron carriers and dissipation of the proton gradient. In our study, F_v/F_m continued to increase beyond 1 h and stabilized after 2 h, indicating that shorter dark periods may make it difficult to distinguish between transient and persistent stress.

Under high light, initial photoinhibition (Figures 5D, F) likely resulted from pre-acclimation to 250 $\mu\text{mol m}^{-2} \text{s}^{-1}$ in the walk-in growth chamber. Plants that had been previously grown under low light were more susceptible to photoinhibition even under moderate intensities (Gjindali and Johnson, 2023). As acclimation progressed, photochemical efficiency improved through the repair mechanism, resulting in ~ 0.83 of F_v/F_m from DAT 4. Under low light, F_v/F_m gradually declined but did not fall below 0.82, suggesting no severe photodamage. Instead, this pattern may reflect a physiological shift toward maximizing light capture (e.g., increasing antenna size), potentially at the expense of electron transport and carbon fixation capacity (Gjindali and Johnson, 2023).

4.2 Temperature and light combination effect on photochemistry

Temperature influenced photochemistry less dynamically than light intensity, yet clear stress responses were observed under suboptimal thermal conditions. Low temperature initially suppressed Φ_{PSII} , mainly due to increased Φ_{NO} rather than Φ_{NPQ} , indicating excess energy loss through non-regulated pathways and photoinhibition. Over time, however, Φ_{PSII} increased substantially as Φ_{NO} decreased, suggesting photosynthetic acclimation. According to previous studies, such recovery under cold stress has been associated with enhanced repair and metabolic adjustments, including reduced antenna size, increased expression

of the cytochrome b_6/f complex and Rubisco, and higher ATP synthase activity, which have been reported to improve electron transport and carbon fixation capacity (Bascañán-Godoy et al., 2012).

Cold stress impairs enzyme activity in the Calvin-Benson cycle and reduces thylakoid membrane fluidity, limiting electron transport and PSII function (Fracheboud and Leipner, 2003). Low qL values under low temperature conditions in this study may indicate an over-reduction of the PQ pool and a potential accumulation of ROS. However, during acclimation, increased qL with decreased Φ_{NO} suggests a shift toward more efficient electron transport and reduced risk of photodamage (Bascañán-Godoy et al., 2012; Mattila et al., 2020). The gradual recovery of F_v/F_m under low temperature stress reflects repair of PSII components such as D1 and cytochrome b_6/f (Bascañán-Godoy et al., 2012; DeEll and Toivonen, 2003).

In contrast, high temperature resulted in the highest qL values but declining F_v'/F_m' and F_v/F_m (Figure 5), suggesting heat-induced inhibition of electron transport despite maintained reaction center openness (Mathur et al., 2014). Heat stress affects PQ oxidation, leading to singlet oxygen accumulation, plastoquinol degradation, and inhibition of Calvin-Benson cycle activity by Rubisco deactivation, thereby disrupting nicotinamide adenine dinucleotide phosphate (NADPH) consumption and redox balance (Rath et al., 2022; Sharkey and Zhang, 2010). These effects can reduce PSII efficiency, with a quadratic decrease in F_v/F_m as temperature increases (Fracheboud and Leipner, 2003; Willits and Peet, 2001).

Notably, combinations of suboptimal light and temperature amplify stress responses. Under low temperatures with high light, Φ_{PSII} was the lowest and Φ_{NO} was the highest, indicating photoinhibition due to excess light energy and limited photochemical capacity (Figures 2B, H). Conversely, high temperature combined with low light also impaired photochemistry (Figure 2A). Under this condition, F_v'/F_m' was particularly reduced, potentially due to limited light harvesting capacity paired with sustained thermal inhibition of photosynthesis and reduced chlorophyll content (Gjindali and Johnson, 2023). While high light can drive photoprotection, low light combined with high temperature reduces chlorophyll content and Calvin cycle enzyme activity, leading to further suppression of photochemical activity (Zhou et al., 2022).

Overall, while high temperatures had limited effects on Φ_{PSII} in this study (Figure 4A), the observed decline in F_v/F_m 8 h (~ 0.81) suggests moderate but persistent stress. Relatively low heat tolerance of lettuce may explain the limited recovery observed, as its acclimation capacity under heat stress is less dynamic compared to cold stress or high light acclimation (Hermida-Carrera et al., 2016; Lu et al., 2017).

4.3 Linking CF data to carbon assimilation and growth

Gas exchange partially tracked CF trends but diverged under temperature extremes. Carbon assimilation followed a parabolic

temperature response, with suppression at both low and high temperatures (Yamori et al., 2014). At 18 °C, Φ_{PSII} was reduced in the early stage (Figure 4A), but A remained similar to 25 °C (Figure 6A), and g_s and C_i showed no strong limitation (Table 2), suggesting that photochemical inhibition at low temperature did not constrain CO_2 fixation. Previous studies have reported that reduced photochemistry under cold conditions can be compensated by lower dark respiration, reduced photorespiration, and sustained chlorophyll levels (Yamori et al., 2014; Zhou et al., 2022). At low temperature, an increased CO_2/O_2 solubility ratio favors Rubisco carboxylation over oxygenation, which is generally associated with reduced photorespiration and helps sustain carbon assimilation efficiency under cold conditions (Sage and Kubien, 2007). From DAT 2 to 7, A slightly declined at both 18 and 25 °C (Table 2) despite stable ETR (Figures 4C, D), indicating possible feedback inhibition due to sink limitation or TPU bottlenecks (Adler et al., 2025). This imbalance between electron transport and carbon fixation likely contributed to the gradual decline in the ETR/ A slope (Figure 7).

In contrast, high temperature induced transient inhibition of carbon assimilation followed by strong recovery. At 32 °C, A was initially suppressed significantly (Figure 6A) despite only slight reductions in Φ_{PSII} (Figure 4A), indicating a temporary decoupling between photochemistry and carbon assimilation. Although g_s , E , and C_i were elevated at 32 °C on DAT 2, A remained suppressed, indicating that carbon assimilation was initially limited by non-stomatal factors such as enhanced photorespiration or reduced Rubisco activity rather than CO_2 diffusion (Sharkey and Zhang, 2010; Yamori et al., 2014). As acclimation progressed, A increased substantially by DAT 7 particularly under the high temperature and high light combination (Figure 6B), coinciding with pronounced increases in g_s and E (Figures 6F, G), which in turn increased the slope of the A vs. ETR relationship (Figure 7). Compared to g_s and E , C_i remained slightly higher under the high temperature but was lower under high light intensity, suggesting that increased CO_2 diffusion through stomatal opening was largely balanced by enhanced carbon assimilation rates. This adaptation was also supported by higher $V_{c,\text{max}}$ and TPU at elevated temperatures with high light combination at DAT 7 (Figure 8), indicating metabolic acclimation of carbon assimilation (Farquhar et al., 1980; Urban et al., 2017). Together, these stomatal and biochemical adjustments led to a disproportionate increase in carbon assimilation relative to photochemical efficiency, resulting in a divergence between A and Φ_{PSII} observed under high temperature conditions.

Biomass and shoot water content revealed a decoupling from photosynthetic rate. Although Φ_{PSII} at 18 °C recovered to levels comparable to 25 °C, and A at 32 °C exceeded that at 25 °C by DAT 7, shoot biomass remained highest at 25 °C (Table 4). This indicates that improved photochemical efficiency or CO_2 assimilation did not necessarily translate into biomass accumulation. This may reflect limitations imposed by downstream processes such as respiratory carbon losses or carbon allocation dynamics (Seydel et al., 2022), although these mechanisms were not directly assessed in this study.

Shoot water content was also reduced under thermal extremes (Table 4), likely due to transpirational loss under heat and impaired water uptake or cell expansion under cold (Yu et al., 2025). High light further decreased water content and increased chlorophyll concentration, consistent with physiological and structural acclimation observed in this study (Zha et al., 2019; Zhou et al., 2022).

Taken together, these results indicate that instantaneous CF parameters and gas exchange responses do not necessarily reflect final growth outcomes. However, cumulative ETR, integrated over the experimental period, emerged as a useful predictor of biomass accumulation independent of temperature (Figure 9). This result indicates that integrating photochemical performance across time retains useful information relevant to biomass accumulation. Previous studies have suggested that the predictive value of CF parameters for crop yield improves when temporal dynamics are incorporated (Moriyuki and Fukuda, 2016). In particular, Moriyuki and Fukuda highlighted the importance of developing a high-resolution, time-course CF measurement system to evaluate the potential of CF-based indices for growth prediction, rather than relying on single time-point observations.

Importantly, the cumulative ETR–biomass relationship identified here was derived from short-term (7-day) experiments under controlled conditions. While these results demonstrate the potential of temporally integrated CF metrics to link photochemical performance with biomass accumulation, further validation over longer growth periods and across different crop species and cultivars is required to assess the broader applicability of this approach.

4.4 High-temporal resolution CF monitoring system for real-time growing condition control

CF offers a comprehensive and reliable method for assessing photochemical efficiency and plant stress responses. Unlike gas exchange measurements, CF provides detailed information on the function of PSII and electron transport, including parameters such as Φ_{PSII} , Φ_{NPQ} , Φ_{NO} , q_L , and F_v/F_m' , which help characterize how different stress conditions affect photosynthetic capacity (Kalaji et al., 2016). These indicators reveal whether stress is transient or sustained, photoinhibitory or protective, which gas exchange measurements alone cannot distinguish. A decline in F_v/F_m is a widely accepted marker of photoinhibition under temperature and light stress (Maxwell and Johnson, 2000). In this study, A recovered over time under the high temperature and high light combination due to increased g_s , but F_v/F_m remained low, indicating sustained photoinhibitory damage that would have been overlooked using CO_2 exchange alone (Willits and Peet, 2001).

Conventional methods for determining F_v/F_m require a long period of dark adaptation, which would interrupt ongoing light treatments if measurements are conducted during the photoperiod (Willits and Peet, 2001), while measurements on detached leaves

may not reflect real-time physiological responses (Yu and Chen, 2023). Instead, parameters such as F_v'/F_m' and qL can provide insights into PSII photochemical efficiency and electron transport limitations (Baker et al., 2007), but they require accurate measurement of F_o' , which can only be obtained when all PSII reaction centers are open and is therefore challenging under ambient light conditions (Kramer et al., 2004). In this study, far-red LED lighting was integrated into the CF monitoring system in the growth chamber (Figure 1), enabling rapid and automated estimation of F_o' and consequently F_v'/F_m' and qL without long dark adaptation or interruption of daytime conditions (Maxwell and Johnson, 2000; Tietz et al., 2017).

Real-time, high-frequency CF monitoring enabled early detection of plant stress and subtle changes over time in photosynthetic performance. Unlike conventional gas exchange measurements, which are typically conducted at daily or less frequent intervals, CF can be collected non-destructively at much higher temporal resolution (Maxwell and Johnson, 2000; Moustaka and Moustakas, 2023). In this study, CF parameters were measured every 30 minutes, enabling the visualization of diurnal patterns and stress dynamics in real-time. This level of detail is critical for detecting rapid photochemical responses and interpreting acclimation processes. The system's flexibility, enabled by serial communication between the chlorophyll fluorometer and the datalogger, allows customized measurement regimes based on experimental objectives (Nam et al., 2025; van Iersel et al., 2016).

Real-time CF data can support adaptive control of growing conditions in CEA systems. CF monitoring systems have the potential to optimize energy use, maximize productivity, and protect plants from environmental stress by responding to photochemical indicators such as Φ_{PSII} and F_v'/F_m' (Ahlman et al., 2017; Baker and Rosenqvist, 2004). In previous studies, CF-based biofeedback systems were used to adjust LED lighting intensity to maintain target ETR or Φ_{PSII} as plant responses changed, reducing energy use while sustaining photosynthetic performance (Nam et al., 2025; van Iersel et al., 2016). For example, based on our results, high light combined with low temperature induced photoinhibition, which could be mitigated by temporarily dimming LED lights. As plants acclimate and recover their photosynthetic efficiency, light intensity can be gradually restored or even increased to promote growth. In vertical farms, continuous lighting with a 24-h photoperiod and spectra with a high blue fraction or ultraviolet (UV) LED lighting are being actively investigated for their effects on crop productivity and quality. Under these conditions, real-time CF monitoring combined with biofeedback light control can be used to diagnose light stress and track acclimation processes, allowing dynamic adjustment of light intensity and spectrum based on photochemical responses. Such plant-driven lighting strategies may help prevent severe photoinhibition while maintaining photosynthetic performance. This approach can also be extended to a comprehensive CEA environmental control system using CF parameters to regulate not only lighting but also temperature, ventilation, and irrigation, applicable in both vertical farming systems and greenhouses (Nam et al., 2025; van Iersel et al., 2016).

5 Conclusion

This study applied high-temporal resolution CF monitoring to evaluate photosynthetic responses to varying light and temperature conditions. High light and low temperature stress initially reduced PSII efficiency, but gradual acclimation over one week was observed, indicated by decreases in Φ_{NO} and increases in F_v'/F_m' , rather than by changes in NPQ. In contrast, high temperature with high light increased CO_2 assimilation markedly over time due to enhanced stomatal conductance, yet F_v'/F_m' remained suppressed, suggesting sustained photoinhibition. The high-frequency CF monitoring system, operating every 30 minutes, enabled the real-time detection of subtle changes and diurnal trends in photochemical responses, capturing stress responses and acclimation patterns that would not have been evident from daily measurements or gas exchange data alone. The integration of light-adapted parameters requiring far-red illumination, such as qL and F_v'/F_m' , allowed for a more comprehensive interpretation of photochemical limitations and electron transport efficiency. Although CF parameters did not always align with downstream carbon assimilation or biomass accumulation, they provided valuable insights into photochemical bottlenecks and stress status. These findings highlight the potential of CF monitoring to support real-time environmental decision-making in CEA systems, for example, by identifying photochemical stress thresholds that could inform adaptive adjustments in supplemental light intensity or thermal management.

Data availability statement

The raw data supporting the conclusions of this article will be made available by the authors, without undue reservation.

Author contributions

SN: Visualization, Investigation, Validation, Conceptualization, Formal analysis, Writing – original draft, Data curation, Methodology. RF: Funding acquisition, Project administration, Resources, Writing – review & editing, Validation, Supervision, Visualization.

Funding

The author(s) declared that financial support was received for this work and/or its publication. This research was funded by the USDA-NIFA-SCRI, award number 2018-51181-28365, project “LAMP: Lighting approaches to maximize profits”, USDA AFRI FAS Program A1521 5a, award number 2026-67021-45822, project “Chlorophyll fluorescence-based biofeedback system to control LED lighting in greenhouses and vertical farms”, the Department of Horticulture, the College of Agricultural and Environmental

Sciences, and the Office of the Senior Vice President for Academic Affairs and Provost.

Acknowledgments

We are deeply indebted to the late Professor Dr. Marc W. van Iersel, who provided the initial conceptualization and experimental-design framework for this study. We thank the Horticultural Physiology and the CEA Crop Physiology and Production Laboratories for the technical support and Dr. Cari Peters and JR Peters for fertilizer donation.

Conflict of interest

The author(s) declared that this work was conducted in the absence of any commercial or financial relationships that could be construed as a potential conflict of interest.

The author RF declared that they were an editorial board member of *Frontiers*, at the time of submission. This had no impact on the peer review process and the final decision.

Generative AI statement

The author(s) declared that generative AI was used in the creation of this manuscript. ChatGPT (GPT-4, June 2025 version;

OpenAI, San Francisco, CA, USA) was used to help edit the language and readability of the manuscript, and DALL-E 3 (OpenAI, accessed via ChatGPT in June 2025) was used to draft schematic elements of [Figure 1](#). All AI-assisted content was thoroughly reviewed, edited, and verified by the authors, who take full responsibility for the published material.

Any alternative text (alt text) provided alongside figures in this article has been generated by *Frontiers* with the support of artificial intelligence and reasonable efforts have been made to ensure accuracy, including review by the authors wherever possible. If you identify any issues, please contact us.

Publisher's note

All claims expressed in this article are solely those of the authors and do not necessarily represent those of their affiliated organizations, or those of the publisher, the editors and the reviewers. Any product that may be evaluated in this article, or claim that may be made by its manufacturer, is not guaranteed or endorsed by the publisher.

Supplementary material

The Supplementary Material for this article can be found online at: <https://www.frontiersin.org/articles/10.3389/fpls.2026.1733839/full#supplementary-material>

References

- Adler, S. O., Kitashova, A., Bulović, A., Nägele, T., and Klipp, E. (2025). Plant cold acclimation and its impact on sensitivity of carbohydrate metabolism. *NPJ Syst. Biol. Appl.* 11, 28. doi: 10.1038/s41540-025-00505-1
- Ahlman, L., Bänkestad, D., and Wik, T. (2017). Using chlorophyll a fluorescence gains to optimize LED light spectrum for short term photosynthesis. *Comput. Electron. Agric.* 142, 224–234. doi: 10.1016/j.compag.2017.07.023
- Baker, N. R., Harbinson, J., and Kramer, D. M. (2007). Determining the limitations and regulation of photosynthetic energy transduction in leaves. *Plant Cell Environ.* 30, 1107–1125. doi: 10.1111/j.1365-3040.2007.01680.x
- Baker, N. R., and Rosenqvist, E. (2004). Applications of chlorophyll fluorescence can improve crop production strategies: an examination of future possibilities. *J. Exp. Bot.* 55, 1607–1621. doi: 10.1093/jxb/erh196
- Bascuñán-Godoy, L., Sanhueza, C., Cuba, M., Zuñiga, G. E., Corcuera, L. J., and Bravo, L. A. (2012). Cold-acclimation limits low temperature induced photoinhibition by promoting a higher photochemical quantum yield and a more effective PSII restoration in darkness in the Antarctic rather than the Andean ecotype of *Colobanthus quitensis* Kunt Bartl (Cariophyllaceae). *BMC Plant Biol.* 12, 1–15. doi: 10.1186/1471-2229-12-114
- Bruce, T. J., Matthes, M. C., Napier, J. A., and Pickett, J. A. (2007). Stressful “memories” of plants: evidence and possible mechanisms. *Plant Sci.* 173, 603–608. doi: 10.1016/j.plantsci.2007.09.002
- DeEll, J. R., and Toivonen, P. M. (2003). *Practical applications of chlorophyll fluorescence in plant biology* (Norwell, MA, USA: Springer Science & Business Media).
- Farquhar, G. D., von Caemmerer, S. V., and Berry, J. A. (1980). A biochemical model of photosynthetic CO₂ assimilation in leaves of C₃ species. *Planta* 149, 78–90. doi: 10.1007/BF00386231
- Faust, J. E., and Logan, J. (2018). Daily light integral: A research review and high-resolution maps of the United States. *HortScience* 53, 1250–1257. doi: 10.21273/HORTSCI13144-18
- Fracheboud, Y., and Leipner, J. (2003). “The application of chlorophyll fluorescence to study light, temperature, and drought stress,” in *Practical applications of chlorophyll fluorescence in plant biology* (Springer), 125–150. doi: 10.1007/978-1-4615-0415-3_4
- Genty, B., Briantais, J. M., and Baker, N. R. (1989). The relationship between the quantum yield of photosynthetic electron transport and quenching of chlorophyll fluorescence. *Biochim. Biophys. Acta (BBA)-General Subj.* 990, 87–92. doi: 10.1016/S0304-4165(89)80016-9
- Gjindali, A., and Johnson, G. N. (2023). Photosynthetic acclimation to changing environments. *Biochem. Soc. Trans.* 51, 473–486. doi: 10.1042/BST20211245
- Haworth, M., Marino, G., Atzori, G., Fabbri, A., Daccache, A., Killi, D., et al. (2023). Plant physiological analysis to overcome limitations to plant phenotyping. *Plants* 12, 4015. doi: 10.3390/plants12234015
- Hermida-Carrera, C., Kapralov, M. V., and Galmés, J. (2016). Rubisco catalytic properties and temperature response in crops. *Plant Physiol.* 171, 2549–2561. doi: 10.1104/pp.16.01846
- Holmes, S. C., Wells, D. E., Pickens, J. M., and Kemble, J. M. (2019). Selection of heat tolerant lettuce (*Lactuca sativa* L.) cultivars grown in deep water culture and their marketability. *Horticulturae* 5, 50. doi: 10.3390/horticulturae5030050
- Hussain, S. S. (2019). Toward understanding the regulation of photosynthesis under abiotic stresses: recent developments. *Photosynthesis Productivity Environ. Stress*, 135–162. doi: 10.1002/9781119501800.ch8
- Janda, T., Prerostová, S., Vanková, R., and Darkó, É. (2021). Crosstalk between light- and temperature-mediated processes under cold and heat stress conditions in plants. *Int. J. Mol. Sci.* 22, 8602. doi: 10.3390/ijms22168602
- Kalaji, H. M., Jajoo, A., Oukarroum, A., Brestic, M., Zivcak, M., Samborska, I. A., et al. (2016). Chlorophyll a fluorescence as a tool to monitor physiological status of plants under abiotic stress conditions. *Acta physiologiae plantarum* 38, 1–11. doi: 10.1007/s11738-016-2113-y
- Kramer, D. M., Johnson, G., Kiirats, O., and Edwards, G. E. (2004). New fluorescence parameters for the determination of QA redox state and excitation energy fluxes. *Photosynthesis Res.* 79, 209–218. doi: 10.1023/B:PRES.0000015391.99477.0d

- Liu, J., and van Iersel, M. W. (2021). Photosynthetic physiology of blue, green, and red light: Light intensity effects and underlying mechanisms. *Front. Plant Sci.* 12. doi: 10.3389/fpls.2021.619987
- Lu, T., Meng, Z., Zhang, G., Qi, M., Sun, Z., Liu, Y., et al. (2017). Sub-high temperature and high light intensity induced irreversible inhibition on photosynthesis system of tomato plant (*Solanum lycopersicum* L.). *Front. Plant Sci.* 8. doi: 10.3389/fpls.2017.00365
- Lysenko, V., D. Rajput, V., Kumar Singh, R., Guo, Y., Kosolapov, A., Usova, E., et al. (2022). Chlorophyll fluorometry in evaluating photosynthetic performance: key limitations, possibilities, perspectives and alternatives. *Physiol. Mol. Biol. Plants* 28, 2041–2056. doi: 10.1007/s12298-022-01263-8
- Mathur, S., Agrawal, D., and Jajoo, A. (2014). Photosynthesis: response to high temperature stress. *J. Photochem. Photobiol. B: Biol.* 137, 116–126. doi: 10.1016/j.jphotobiol.2014.01.010
- Mattila, H., Mishra, K. B., Kuusisto, I., Mishra, A., Novotná, K., Šebela, D., et al. (2020). Effects of low temperature on photoinhibition and singlet oxygen production in four natural accessions of *Arabidopsis*. *Planta* 252, 1–17. doi: 10.1007/s00425-020-03423-0
- Maxwell, K., and Johnson, G. N. (2000). Chlorophyll fluorescence—a practical guide. *J. Exp. Bot.* 51, 659–668. doi: 10.1093/jxb/51.345.659
- Mayorga-Gomez, A. M., van Iersel, M. W., and Ferrarezi, R. S. (2024). Varying light intensities affect lettuce growth and physiology in controlled indoor environments. *Horticulturae* 10, 931. doi: 10.3390/horticulturae10090931
- Moriyuki, S., and Fukuda, H. (2016). High-throughput growth prediction for *Lactuca sativa* L. seedlings using chlorophyll fluorescence in a plant factory with artificial lighting. *Front. Plant Sci.* 7, 394. doi: 10.3389/fpls.2016.00394
- Moustaka, J., and Moustakas, M. (2023). Early-stage detection of biotic and abiotic stress on plants by chlorophyll fluorescence imaging analysis. *Biosensors* 13, 796. doi: 10.3390/bios13080796
- Murchie, E. H., and Niyogi, K. K. (2011). Manipulation of photoprotection to improve plant photosynthesis. *Plant Physiol.* 155, 86–92. doi: 10.1104/pp.110.168831
- Nam, S., van Iersel, M. W., and Ferrarezi, R. S. (2025). Biofeedback control of photosynthetic lighting using real-time monitoring of leaf chlorophyll fluorescence. *Physiologia Plantarum* 177, e70073. doi: 10.1111/ppl.70073
- PPSystems (2022). “High-Speed CO₂ ramping technique: rapid A/Ci curves in minutes,” in *Application note* (PP Systems, Amesbury, MA). Available online at: https://ppsystems.com/wp-content/uploads/AN_CIRAS-4_Rapid-Aci-Curves.pdf.
- Rath, J. R., Pandey, J., Yadav, R. M., Zamal, M. Y., Ramachandran, P., Mekala, N. R., et al. (2022). Temperature-induced reversible changes in photosynthesis efficiency and organization of thylakoid membranes from pea (*Pisum sativum*). *Plant Physiol. Biochem.* 185, 144–154. doi: 10.1016/j.plaphy.2022.05.036
- Sage, R. F., and Kubien, D. S. (2007). The temperature response of C3 and C4 photosynthesis. *Plant Cell Environ.* 30, 1086–1106. doi: 10.1111/j.1365-3040.2007.01682.x
- Sakoda, K., Sakurai, A., and Imamura, S. (2025). Difference in single-leaf and whole-plant photosynthetic response to light under steady and non-steady states in *Arabidopsis thaliana*. *Front. Plant Sci.* 16. doi: 10.3389/fpls.2025.1532522
- Seydel, C., Kitashova, A., Fürtauer, L., and Nägele, T. (2022). Temperature-induced dynamics of plant carbohydrate metabolism. *Physiologia Plantarum* 174, e13602. doi: 10.1111/ppl.13602
- Sharkey, T. D., Bernacchi, C. J., Farquhar, G. D., and Singsaas, E. L. (2007). Fitting photosynthetic carbon dioxide response curves for C3 leaves. *Plant Cell Environ.* 30, 1035–1040. doi: 10.1111/j.1365-3040.2007.01710.x
- Sharkey, T. D., and Zhang, R. (2010). High temperature effects on electron and proton circuits of photosynthesis. *J. Integr. Plant Biol.* 52, 712–722. doi: 10.1111/j.1744-7909.2010.00975.x
- Stinziano, J. R., Morgan, P. B., Lynch, D. J., Saathoff, A. J., McDermit, D. K., and Hanson, D. T. (2017). The rapid A–C_i response: photosynthesis in the phenomic era. *Plant, Cell & Environment* 40, 1256–1262. doi: 10.1111/pce.12911
- Tietz, S., Hall, C. C., Cruz, J. A., and Kramer, D. M. (2017). NPQ (_T): a chlorophyll fluorescence parameter for rapid estimation and imaging of non-photochemical quenching of excitons in photosystem-II-associated antenna complexes. *Plant, Cell & Environment* 40, 1243–1255. doi: 10.1111/pce.12924
- Urban, J., Ingwers, M., McGuire, M. A., and Teskey, R. O. (2017). Stomatal conductance increases with rising temperature. *Plant Signaling Behav.* 12, e1356534. doi: 10.1080/15592324.2017.1356534
- van Iersel, M., and Bugbee, B. (2000). A multiple chamber, semicontinuous, crop carbon dioxide exchange system: design, calibration, and data interpretation. *J. Am. Soc. Hortic. Sci.* 125, 86–92. doi: 10.21273/JASHS.125.1.86
- van Iersel, M. W., Weaver, G., Martin, M. T., Ferrarezi, R. S., Mattos, E., and Haidekker, M. (2016). A chlorophyll fluorescence-based biofeedback system to control photosynthetic lighting in controlled environment agriculture. *J. Am. Soc. Hortic. Sci.* 141, 169–176. doi: 10.21273/JASHS.141.2.169
- Willits, D., and Peet, M. (2001). Measurement of chlorophyll fluorescence as a heat stress indicator in tomato: laboratory and greenhouse comparisons. *J. Am. Soc. Hortic. Sci.* 126, 188–194. doi: 10.21273/JASHS.126.2.188
- Wimalasekera, R. (2019). “Effect of light intensity on photosynthesis,” in *Photosynthesis, productivity and environmental stress* Oxford, UK: Wiley, 65–73. doi: 10.1002/9781119501800.ch4
- Yamori, W., Hikosaka, K., and Way, D. A. (2014). Temperature response of photosynthesis in C₃, C₄, and CAM plants: temperature acclimation and temperature adaptation. *Photosynthesis Res.* 119, 101–117. doi: 10.1007/s11120-013-9874-6
- Yang, Y. N., Le, T. T. L., Hwang, J.-H., Zulfugarov, I. S., Kim, E.-H., Kim, H. U., et al. (2022). High light acclimation mechanisms deficient in a PsbS-knockout *Arabidopsis* mutant. *Int. J. Mol. Sci.* 23, 2695. doi: 10.3390/ijms23052695
- Yu, J.-Y., and Chen, C.-M. (2023). Chlorophyll fluorescence parameter as a tool in selecting heat-tolerant summer-flowering chrysanthemum (*Dendranthema × grandiflorum*). *HortScience* 58, 1603–1609. doi: 10.21273/HORTSCI17361-23
- Yu, M., Luobu, Z., Zhuoga, D., Wei, X., and Tang, Y. (2025). Advances in plant response to low-temperature stress. *Plant Growth Regul.* 105, 167–185. doi: 10.1007/s10725-024-01253-8
- Zha, L., Liu, W., Zhang, Y., Zhou, C., and Shao, M. (2019). Morphological and physiological stress responses of lettuce to different intensities of continuous light. *Front. Plant Sci.* 10. doi: 10.3389/fpls.2019.01440
- Zhou, J., Li, P., and Wang, J. (2022). Effects of light intensity and temperature on the photosynthesis characteristics and yield of lettuce. *Horticulturae* 8, 178. doi: 10.3390/horticulturae8020178
- Zhou, R., Yu, X., Li, X., Dos Santos, T. M., Rosenqvist, E., and Ottosen, C.-O. (2020). Combined high light and heat stress induced complex response in tomato with better leaf cooling after heat priming. *Plant Physiol. Biochem.* 151, 1–9. doi: 10.1016/j.plaphy.2020.03.011
- Zuo, G. (2025). Non-photochemical quenching (NPQ) in photoprotection: insights into NPQ levels required to avoid photoinactivation and photoinhibition. *New Phytol.* 246, 1967–1974. doi: 10.1111/nph.70121